Journal of Quaternary Science

# Mud redeposition during river incision as a factor affecting authigenic 10 Be/ 9 Be dating: Early Pleistocene large mammal fossil-bearing site Nová Vieska, eastern Danube Basin



| | |
|---|---|
| Journal: | *Journal of Quaternary Science* |
| Manuscript ID | JQS-22-0067 |
| Wiley - Manuscript type: | Research Article |
| Date Submitted by the Author: | 03-Jun-2022 |





| | |
|---|---|
| Complete List of Authors: | Šujan, Michal; Univerzita Komenskeho v Bratislave Prirodovedecka fakulta<br>Braucher, Regis; Aix-Marseille Universite<br>Chyba, Andrej; Chemicky ustav Slovenskej akademie vied<br>Vlačiky, Martin; Statny geologicky ustav Dionyza Stura<br>Aherwar, Kishan; Univerzita Komenskeho v Bratislave Prirodovedecka fakulta<br>Rózsová, Barbara; Univerzita Komenskeho v Bratislave Prirodovedecka fakulta<br>Fordinál, Klement; Statny geologicky ustav Dionyza Stura<br>Maglay, Juraj; Statny geologicky ustav Dionyza Stura<br>Nagy, Alexander; Statny geologicky ustav Dionyza Stura<br>Moravcová, Martina; Statny geologicky ustav Dionyza Stura<br>Team, ASTER; Aix-Marseille Universite |





| | |
|---|---|
| Keywords: | cosmogenic nuclides, authigenic beryllium, facies analysis, wandering river, redeposition |
| | |

# Mud redeposition during river incision as a factor affecting authigenic $^{10}Be/^{9}Be$ dating: Early Pleistocene large mammal fossil-bearing site Nová Vieska, eastern Danube Basin

Michal Šujan[1,*], Régis Braucher[2], Andrej Chyba[3], Martin Vlačiky[4], Kishan Aherwar[1], Barbara Rózsová[1], Klement Fordinál[4], Juraj Maglay[4], Alexander Nagy[4], Martina Moravcová[4], Aster Team[2]

1 – Department of Geology and Paleontology, Faculty of Natural Sciences, Comenius University in Bratislava, Ilkovičova 6, 842 15 Bratislava, Slovakia; michal.sujan@uniba.sk; ORCID: 0000-0001-7933-8669; kishanaherwar2@gmail.com; rozsova9@uniba.sk

2 – CNRS-IRD-Collège de France-INRA, CEREGE, Aix-Marseille Univ., 13545 Aix-en-Provence, France ; braucher@cerege.fr; aumaitre@cerege.fr

3 – Institute of Chemistry, Slovak Academy of Sciences, Dúbravská cesta 9, 845 38 Bratislava, Slovakia; andrej.chyba@savba.sk

4 – State Geological Institute of Dionýz Štúr, Mlynská dolina 1, 817 04 Bratislava 11, Slovakia; martin.vlaciky@gmail.com; klement.fordinal@geology.sk; juraj.maglay@geology.sk; alexander.nagy@geology.sk; martina.moravcova@geology.sk

* – corresponding author

## Abstract

This study examines the suitability of the authigenic $^{10}Be/^{9}Be$ dating method to the dating of the deposits of an incising river, taking as an example the Nová Vieska river terrace, which accumulated during the neotectonic inversion of the Danube Basin (western Slovakia). The succession was formed by a wandering river with minor preservation of proximal floodplain muds. The frequent occurrence of mud intraclasts reflects a significant input of eroded material from underlying, older successions. The ages of 13 authigenic $^{10}Be/^{9}Be$ dating samples formed three groups: (1) samples from below the base of the river terrace yielded dates of ~4.13–3.70 Ma; (2) muddy intraclasts from the river terrace an age range of ~2.79–1.96 Ma; and (3) *in situ* muddy layers had ages in the range of ~1.91–1.39 Ma. The large mammal fossil assemblage from channel thalweg deposits yielded a biostratigraphic age of ~3.6–2.2 Ma, matching the age of intraclasts, and thus emphasizing the redeposited origin of those fossils. The relatively wide range of authigenic $^{10}Be/^{9}Be$ dating ages is interpreted as a result of the redeposition of mud from older strata on three scales: decimeter-scale intraclasts, millimeter-scale rip-up clasts mixed into the newly formed beds, and formation of two authigenic rims with different age and $^{10}Be/^{9}Be$ record around individual particles. Considering these observations, an age range of *in situ* layers of ~1.91–1.39 Ma is proposed as the depositional age of the river terrace. The effect of redeposition is thus shown to be potentially limiting to the application of authigenic $^{10}Be/^{9}Be$ dating to incising rivers, and stands in marked contrast with aggrading river settings, where redeposition of older sediment is limited and the degree of $^{10}Be/^{9}Be$ variability is low.

**Key words:** cosmogenic nuclides, authigenic beryllium, facies analysis, wandering river, redeposition

# 1. Introduction

The authigenic $^{10}Be/^{9}Be$ dating method allows the dating of the deposition of a clay-bearing sediment, provided that certain conditions are fulfilled (Bourlès et al., 1989; Lebatard et al., 2008; Šujan et al., 2016; Simon et al., 2020). Despite this great potential to establish depositional ages for the most common type of sediment on Earth (Schieber, 1998), the limits of this method in continental environments are still not fully appreciated. The complexity of the factors which may possibly affect the method arises from the different sources of the two isotopes employed in the system, as the radionuclide $^{10}Be$ is produced in the atmosphere by cosmic rays, while the stable isotope $^{9}Be$ is derived from the weathering of rocks. Both isotopes may then be mixed in a water column and incorporated into the authigenic phase on the surface of sediment particles (Bourlès et al., 1989; Willenbring and von Blanckenburg, 2010; Wittmann et al., 2017; Bernhardt et al., 2020).

It has been shown that sedimentary successions accumulated in endorheic lacustrine basins located in a craton setting with low tectonic activity and stable provenance, such as the Chad Basin in Africa, are highly suited to the employment of the method (Lebatard et al., 2008; Lebatard et al., 2010; Novello et al., 2015). Although located in the more challenging conditions of an Alpine orogenic belt, the Danube Basin has also proven to be suitable for dating using authigenic $^{10}Be/^{9}Be$, especially the alluvial sequences found in the Basin, thanks to the high accommodation to sediment supply rate (Šujan et al., 2016; Šujan et al., 2020). On the other hand, the alluvial succession in the Upper Thrace Depression, Bulgaria, displays a high degree of authigenic $^{10}Be/^{9}Be$ variability, preventing the effective application of the method (Schaller et al., 2015), a result likely due to the significant tectonic activity of the pull-apart basins in this extensional province (Burchfiel et al., 2000).

This study aims to widen the knowledge of the applicability of authigenic $^{10}Be/^{9}Be$ dating to alluvial sediments. A key hypothesis which needs to be tested is the assumption that one of the major factors affecting the beryllium isotopic ratio appears to be the redeposition of older sediments, a phenomenon which occurs when a river recycles its own floodplain during incision and older mud particles are incorporated into newly formed strata. Whereas the continuous growth of authigenic rims records the changing $^{10}Be/^{9}Be$ ratio in a water column (Wittmann et al., 2017), a shift in isotopic ratio might be caused by the different ages of the authigenic rim formation, associated with the process of the redeposition of older mud particles.

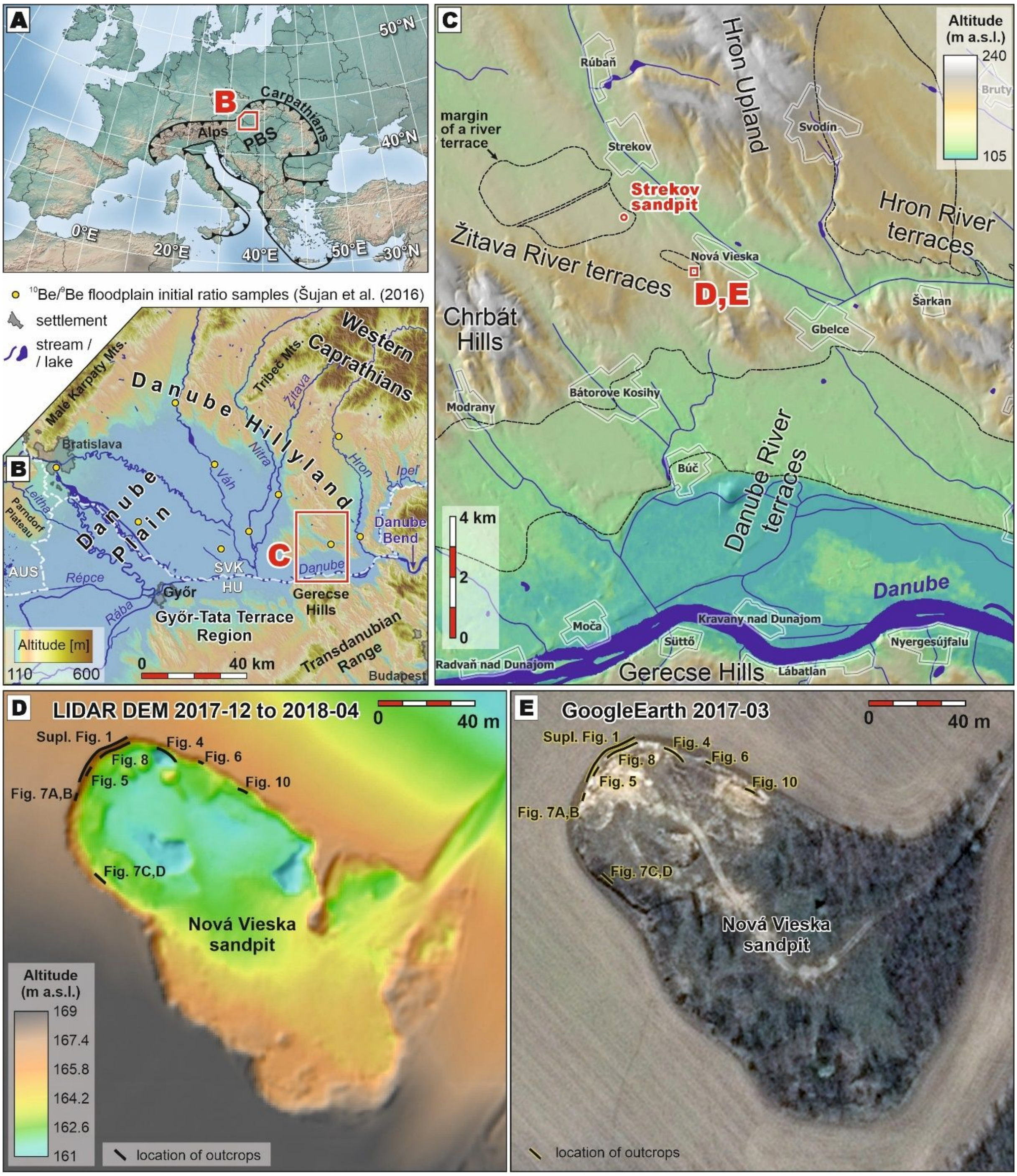


Fig. 1. Location of the study area. (A) Location of the Danube Basin within the Alpine-Carpathian orogenic belt. PBS – Pannonian Basin System (B) General topography of the Danube Basin and the present river network, with distribution of the samples used for calculation of the alluvial initial $^{10}$Be/$^{9}$Be ratio in Šujan et al. (2016). (C) Topographic map of the vicinity of the Nová Vieska site with the margins of the river terraces of the rivers Danube, Hron and Žitava marked. (D)

Lidar digital elevation model of the Nová Vieska sandpit showing the position of sampled outcrops. (E) GoogleEarth image of the Nová Vieska sandpit showing the position of sampled outcrops.

The Nová Vieska river terrace in the eastern Danube Basin (Slovakia) was selected for this study (Vlačiky et al., 2008; Vlačiky et al., 2017) (Fig. 1). An Early Pleistocene age for the locality could be assumed on the basis of the wealth of large mammal fossils which had accumulated in coarse clastic channel-fill deposits. The succession was formed during inversion of the basin, when the river gradually incised into its older alluvial sediments, along with the formation of river terrace staircases (Šujan and Rybár, 2014; Ruszkiczay-Rüdiger et al., 2018; Ruszkiczay-Rüdiger et al., 2020; Šujan et al., 2021). A detailed sedimentological analysis was performed with the goal of discovering any association between the observed authigenic $^{10}Be/^{9}Be$ variability and the processes of alluvial mud redeposition in the river channel during the incision.

## 2. Geological setting

The Danube Basin is the northwesternmost depocenter of the Pannonian Basin System (Fig. 1A), and is surrounded by the Eastern Alps, Western Carpathians and the Transdanubian Range (Fig. 1A, B). It experienced four rifting phases during the period ~16.0–9.5 Ma, with the last one giving rise to Lake Pannon in the region during the Late Miocene (Magyar et al., 1999; Kováč et al., 2011; Magyar et al., 2013; Sztanó et al., 2016; Šujan et al., 2021)(Fig. 2). The regression of Lake Pannon, caused by the progradation of deltaic to shelf slope depositional systems from the northwest to southeast (Magyar et al., 2013), gradually led to the dominance of the alluvial deposition of the Volkovce Formation. The condition of a high accommodation rate to sediment supply ratio during sedimentation led to a high content of muddy floodplain facies, reaching 50–80% (Šujan et al., 2020).

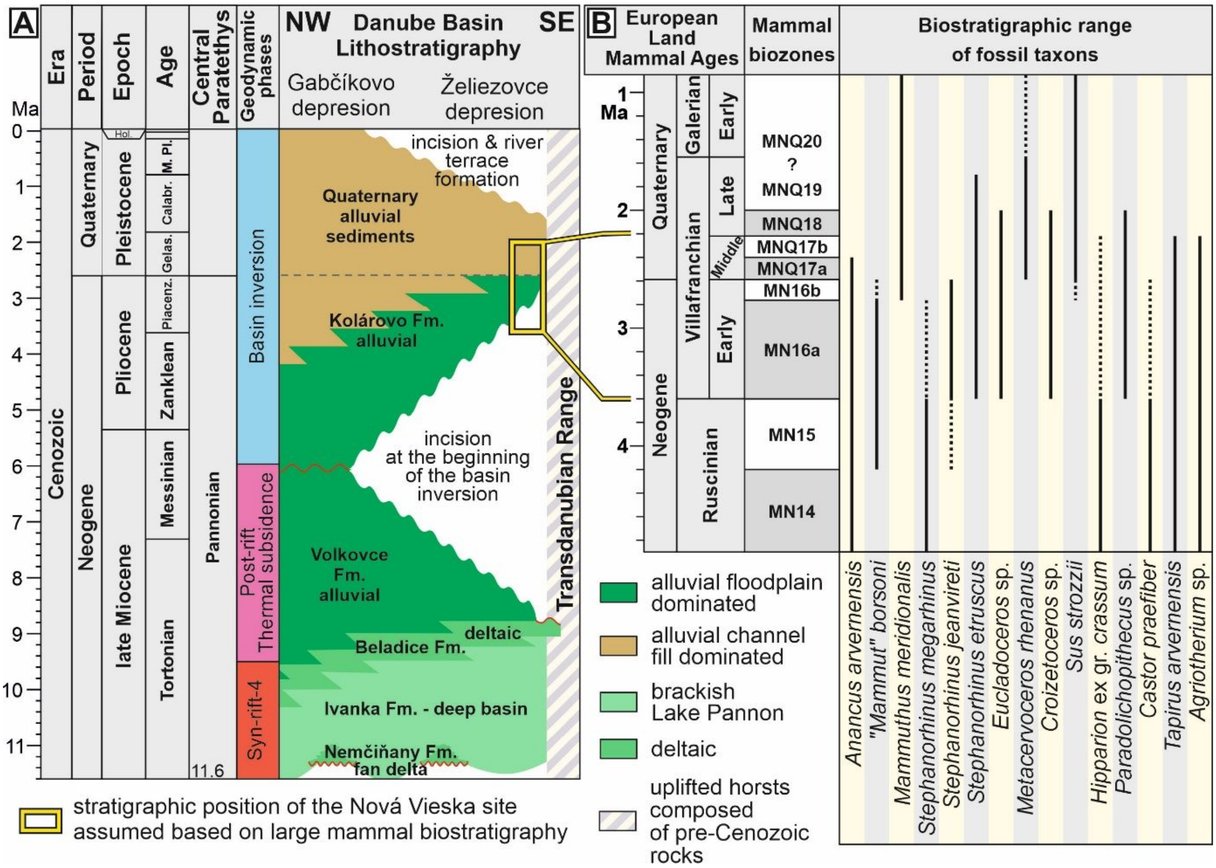


Fig. 2A. Stratigraphy of the eastern Danube Basin indicating the position of studied Nová Vieska site (Sztanó et al., 2016; Šujan et al., 2021). The studied succession was deposited during incision into thick underlying alluvial deposits, formed by the same rivers. B. Biostratigraphic range of the fossil mammal assemblage documented at the Nová Vieska site. See the text for references. The Mammal Neogene and Quaternary zones (MN and MNQ zones) according to Rook and Martínez-Navarro (2010), Hilgen et al. (2012), Raffi et al. (2020) and Paquette et al. (2021).

The floodplain-dominated sedimentation of the Volkovce Fm. ceased at ~6 Ma, when the basin inversion started (Tari, 1994; Vakarcs et al., 1994; Horváth, 1995; Horváth et al., 2006; Tari et al., 2020; Šujan et al., 2021). The basin inversion caused a significant decrease in accommodation rates, uplift and partial denudation of the basin margins and subsidence of the central depression of the basin (Šujan et al., 2018) (Fig. 2). The syn-inversion alluvial deposition of the Kolárovo Formation gradually expanded outwards from the central depression later on, and reached the margins of the basin at ~4–3 Ma (Ruszkiczay-Rüdiger et al., 2020; Šujan et al., 2021). The uplift of the margins overtook the base-level rise after ~3 Ma, and river terraces started to form coevally with incision into the underlying alluvial Kolárovo Fm. and Volkovce Fm. (Šujan et al., 2021) (Fig. 2). One of the oldest sedimentary bodies deposited during this phase of the basin evolution is the Nová Vieska river terrace, investigated in this study. Base-level fall and low accommodation conditions led to the prevailing deposition of coarse-grained channel-fill facies in the regime of a wandering river in the Nová Vieska succession (Vlačiky et al., 2008). The uplift of the area continues in the present day, placing a constraint on active alluvial deposition, confining it mainly to the central depression of the basin (Fig. 1C). The Nová Vieska terrace is therefore in the middle of three terrace river systems, with the Hron River stepping back to the east, the Žitava to the northwest and the Danube to the south (Fig. 1C).

The Nová Vieska sandpit is located in an altitude range of 161 to 168 m a.s.l. (Fig. 1D), ca. 60 m above the water level of the present Danube River. The river terrace succession attains relatively low thickness not exceeding ~6 m. The walls facing northeast, southeast and southwest are excavated actively, mostly due to the regular paleontological investigations (Fig. 1D, E). The river terrace deposits have accumulated above the muds and sands of the floodplain-dominated Volkovce Fm. of Late Miocene age (Vlačiky et al., 2008; Šujan and Rybár, 2014; Šujan et al., 2020).

# 3. Large mammal biostratigraphy

The mammal fossil remnants appear as disarticulated clasts in strata characterized by massive coarse-grained sand and granules with pebbles and with a high abundance of muddy intraclasts (lithofacies SGpm – see facies analysis). Despite their disarticulated nature, the degree of polishing of the surface of the fossils is generally low and uneven.

The paleontological research of the Nová Vieska site is closely related to the investigations of the Strekov site, located nearby (Fig. 1C), and considered analogous in terms of biostratigraphy (Schmidt and Halouzka, 1970). Findings from the Strekov site include rhinoceroses identified as *Coelodonta antiquitatis* (probably incorrect determination - Harčár and Schmidt, 1965), *Stephanorhinus megarhinus* (Schmidt and Halouzka, 1970) and *Stephanorhinus jeanvireti* (Holec, 1986). Evidence of the occurrence of proboscideans includes teeth of *Zygolophodon borsoni*, *Anancus arvernensis* and *Archidiskodon planifrons* (Schmidt and Halouzka, 1970), though this was later redefined as *Archidiskodon meridionalis* (Schmidt, 1977). The presence of cervid taxon *Alces alces* (actually, probably an incorrect determination - Harčár and Schmidt, 1965); the presence of *Cervus* and *Alces* was based on finding mandibles and fragments of antlers. A fossil horn was identified as belonging to the genus *Bison* (Schmidt and Halouzka, 1970) and one mandible to the species *Sus scrofa* (again, probably an incorrect determination - Harčár and Schmidt, 1965). Holec (1986) also mentions two species of beaver – *Trogontherium minus* and *Castor fiber* from the Strekov site.

The first taxa described exclusively from the Nová Vieska locality are two species of rhinoceros – *Stephanorhinus jeanvireti* and *Stephanorhinus etruscus etruscus* (Holec, 1986). On the basis of the relatively short distances between the Strekov and Nová Vieska sand pits and their similar faunal composition Holec (1996) assumed that the fossil remnants were redeposited by the erosion of a single stratigraphic horizon. Holec (1996) extended the previously published descriptions of the taxa from both sites with *Libralces, Hipparion* and *Pliocrocuta perrieri,* but did not specify the location of the finds.

More recent publications deal with the Nová Vieska findings only. Vlačiky et al. (2008) documented the occurrence of teeth from *Mammut borsoni*, *Anancus arvernensis* and *Mammuthus meridionalis*. Moreover, Vlačiky et al. (2010) confirmed the occurrence of three distinct fossil proboscideans at the Nová Vieska site based on micromorphology of tusks. Three species of rhinoceros (*Stephanorhinus megarhinus, S. jeanvireti, S. etruscus etruscus*) were described from the locality (Vlačiky et al., 2008). The teeth of *Stephanorhinus jeanvireti* were subjected to isotopic analyses of carbon and oxygen for paleoclimatic research (Kovács et al., 2015). The cervid findings were specified by Vlačiky et al. (2008) as *Metacervoceros rhenanus*, *Eucladoceros* and *Croizetoceros,* and the authors included a description of *Sus strozzii*. A third lower molar of the primate genus *Paradolichopithecus* was documented by Vlačiky (2009) and Vlačiky et al. (2009). A morphological study of the hipparion teeth allowed a more precise determination to be made, the conclusion being that they belonged to *Hipparion ex gr. crassum* (Vlačiky et al., 2010). Fossil beaver teeth were determined as being from *Castor* cf. *praefiber* (Vlačiky et al., 2010). The fossil remnants of carnivores were extended to include a bear genus *Agriotherium*, and two fragments of teeth proved the occurrence of *Tapirus arvernensis* (Vlačiky et al., 2013).

Some earlier biostratigraphic assumptions are based on findings of both Strekov and Nová Vieska sites together. The redeposited nature of the fossil fauna accumulation had already been recognized by Harčár and Schmidt (1965). Schmidt and Halouzka (1970) suggested two sources of the fossil remnants, the first of which had an early Villafranchian age (MN16) and had undergone a short transport, while the second was of a middle Villafranchian age (MN17) and considered to be *in situ*. Holec (1996) assumed the origin of the findings from Strekov and Nová Vieska in three faunistic complexes: (1) Pliocene age with *Stephanorhinus megarhinus, S. jeanvireti, Hipparion sp.* and "*Mammut*" *borsoni*; (2) Plio-Pleistocene age including *Trogontherium sp., Pliocrocuta perrieri, Stephanorhinus etruscus etruscus, Anancus arvernensis* and *Archidiskodon meridionalis*; and (3) the late Early Pleistocene age with *Bos/Bison* and *Sus scrofa*. Consideration of the most up to date list of fossil fauna (Fig. 2B) presented in the publications referred to and the stratigraphic settings of the fossiliferous layers imply that (1) redeposition led to accumulation of the fossil remnants, and that (2) the assemblage represents a mix of taxa included in the MN16 and MN17 mammal biostratigraphic zones with an age range of 3.6–2.2 Ma (Hilgen et al., 2012; Raffi et al., 2020; Paquette et al, 2021).

# 4. Methods

## 4.1 Sedimentology

A detailed facies analysis of the locality was performed by Vlačiky et al. (2008); nevertheless, continuous excavations have led to exposure of new sedimentary bodies, allowing the verification of certain previous assumptions concerning the sedimentology of the site. The sedimentological logging and mapping of the of facies distribution on the vertical outcrop walls was performed with two aims: (1) to interpret the depositional processes and asses the character of sedimentary environment, and (2) to record the facies character of the strata sampled for dating precisely, in order to understand any variability in depositional processes that may affect the dating result. The field campaign and sampling were conducted during the years 2015, 2016 and 2017. The standard facies analysis of clastic sediments included the description of grain size, structure, texture, geometry and size of the strata, and visualization of the information gained in logs and schemes (Stow, 2005; Miall, 2006). Paleocurrent directions of cross-strata were measured to evaluate the character of accretion of alluvial bars (Almeida et al., 2016); specific data are not, however, presented due to the mainly geochronological focus of the study.

## 4.2 Authigenic $^{10}Be/^{9}Be$ dating

### 4.2.1 Principles of the method

The authigenic beryllium dating employed is based on the measurement of the $^{10}Be/^{9}Be$ ratio, the stable nuclide $^{9}Be$ originating from chemical weathering of rocks, while the radioactive nuclide $^{10}Be$ being produced by secondary cosmic rays in the atmosphere via a process of a spallation reaction on oxygen and nitrogen (Dunai, 2010). Being very reactive, the $^{10}Be$ gets adsorbed into aerosols and is transferred to the Earth surface in soluble form by precipitation (Raisbeck et al., 1981). $^{10}Be$ is removed from the water column in aqueous settings and is incorporated in the authigenic phase, composed mostly of amorphous oxy-hydroxides, which cover the surface of sedimentary particles (Bourlès et al., 1989). The half-life of $^{10}Be$, 1.387 ± 0.012 Ma (Chmeleff et al., 2010; Korschinek et al., 2010), offers the possibility of dating the authigenic phase and, hence, the deposition of sediments within an age range of 0.2 to 14 Ma (Ku et al., 1982; Bourlès et al., 1989; Lebatard et al., 2008), providing that the systems being thus dated are chemically closed.

The age calculation is based on the radioactive decay of an initial concentration that follows the equation: $N_{(t)}=N_0e^{-\lambda t}$, where $N_{(t)}$ is the authigenic $^{10}Be/^{9}Be$ ratio measured in the sample to be dated, $N_0$ is the initial authigenic $^{10}Be/^{9}Be$ ratio, $\lambda$ is the $^{10}Be$ radioactive decay constant, and t is the time elapsed since deposition. This equation makes the essential need to establish the initial isotopic ratio apparent; this, in turn, depends on several factors, such as the lithology of the drainage basin, denudation intensity, the latitude of the study area, depositional environment conditions and the proximity of the source of sediment to the place of deposition (Brown et al., 1992; Graham et al., 2001; Graly et al., 2010; Wittmann et al., 2012; Wittmann et al., 2017). Thus, the initial isotopic ratio might be established by the analysis of samples taken from the same basin and in similar depositional conditions as the dated samples, which are either of an age in the range 0–200 ka and assumed to be contemporary, or of an independently determined age, and the time elapsed is included in the calculation of the initial ratio. The analysis of a set of Holocene floodplain samples distributed across the Danube Basin (Fig. 1B) yielded authigenic $^{10}Be/^{9}Be$ values with a relatively low degree of variability, and this allowed the calculation of the initial ratio for the alluvial deposits used in this study: $4.14 \pm 0.17 \times 10^{-9}$ (Šujan et al., 2016). It should, of course, be noted that this ratio is assumed to have remained stable through time.

**4.2.2 Sampling strategy and sample processing**

Two factors made the decision to apply authigenic $^{10}Be/^{9}Be$ dating to the Nová Vieska river terrace reasonable: (1) in the context of the expected age of ~1.8–2.6 Ma the limited thickness of the accumulation, at only <6 m, may be expected to have caused saturation of the *in situ* cosmogenic nuclide production, thus giving only a minimum exposure age, and (2) a relatively frequent presence of muddy alluvial strata within the sandy-gravelly succession, rendering the whole suitable for the application of the method.

The samples for the authigenic $^{10}Be/^{9}Be$ dating were collected sequentially during the years 2015, 2016 and 2017, as new sedimentary units were exposed by continuous excavation. The sampling was focused on the muddy alluvial strata deposited either as overbank fines, or as oxbow lake fills or muddy accretion on bars. All these types of sampled facies are denoted here as *in situ* strata, and yielded 8 samples. In addition to the *in situ* strata, three samples were taken from redeposited intraclasts of alluvial mud. The lithology of the sampled intraclasts was, on visual inspection, comparable to that of the *in situ* layers. The strata, from which *in situ* as well as intraclast samples originate, are considered to represent the single succession of a river terrace. Two samples were taken from the thick, muddy horizon, which appeared below the base of the river terrace.

The six samples taken in 2015 (first group) were processed at CEREGE, Aix-en-Provence (France), while the seven samples taken in the following years, 2016 and 2017, (second group) underwent processing in the laboratory of the Department of Geology and Paleontology, Faculty of Natural Sciences, Comenius University in Bratislava (Slovakia). The workflow applied at both laboratories followed the methodology described by Bourlès et al. (1989) and Carcaillet et al. (2004). The authigenic phase was extracted from powdered samples using a leaching solution of acetic acid, hydroxilamonium hydrochloride and demineralized water. Aliquots taken from the resulting solution were analyzed to determine the concentrations of $^{9}$Be using atomic adsorption spectrometry (AAS – first group) and by inductively coupled plasma mass spectrometry (CP-MS – second group). The replicability and consistency of both approaches was tested, with positive results. The subsequent processing involved the addition of 300 mg (first group) or 450 mg (second group) of the Scharlau beryllium ICP standard solution (1000 ppm) with $^{10}$Be/$^{9}$Be ratios in the range of 6–8 × $10^{-15}$ (Merchel et al., 2021). Samples were evaporated and resin chemistry was applied to separate beryllium from other elements present in the authigenic phase (Merchel and Herpers, 1999). The purified samples were oxidized at 700°C for one hour in an oven, mixed with niobium powder then transferred to copper cathodes for accelerator mass spectrometer (AMS) measurements. AMS measurements of $^{10}$Be/$^{9}$Be isotopic ratios were carried out at the French national facility ASTER (CEREGE, Aix-en-Provence, France). The AMS $^{10}$Be/$^{9}$Be ratios of all samples reached values at least two orders of magnitude higher when compared to the two processing blanks, and were normalized to their isotopic ratios. The calculated ages with one σ uncertainties were statistically processed using the KDX application – see Fig. 3 (Spencer et al., 2017).

# 5. Results

## 5.1 Facies analysis

Descriptions of the eight facies distinguished, their internal fabric, geometry and inferred depositional processes are included in Table 1. The depositional record exhibits a prevailing coarse-grained nature, with the alternation of sandy-gravelly and sandy units. *In situ* muddy strata represent <15% of the documented succession. Lithofacies SGpm, St and Stb comprise the greater part of the volume, reaching a proportion of ca 60–70% (Figs. 4–7). Lithofacies Sl is common, forming up to 20% locally (Fig. 4), while lithofacies Sr is rare and appears in thin horizons or lenses of only a few centimeters (Fig. 5). All lithofacies are frequently arranged in inclined units of variable lithology 0.5 to 2.5 m thick (Figs. 4–7).

Beside the primary structures summarized in Table 1, the locality Nová Vieska displays a wide range of penecontemporaneous deformations. Fig. 8 shows a large involution structure (Vandenberghe, 2013), reaching a thickness of >3 m in the lower part of the outcrop. The deformation partly preserves original structures, since rotated trough cross-bedding is observable in a number of horizons in Fig. 8E. The involution of strata caused the sub-vertical orientation of the remnants of the primary bedding locally (Fig. 8F). The large involution is associated with decimeter-scale graben-like brittle collapse features, bounded by small faults, but also displaying bending at the margins (Fig. 8G). The involution structure is cut by an erosional surface, while the overlying facies of Stb and St are undeformed.

Sand wedges reaching a height of 5–20 cm comprise relatively common deformations (Fig. 9A). The deformation is limited in the lower part, and includes the bending of the surrounding strata and filling of the wedge by the overlying strata. The symmetrical, rounded downwards bending of the strata on a scale ranging from a few cm to 15 cm is observed rarely with decreasing intensity of deformation towards the base (Fig. 9B). Another type of less frequently observed structure which interrupts the primary bedding is comprised of simple pocket-like burrows filled with sand derived from the overlying strata (Fig. 9C). The structure on the left in Fig. 9C appears to have been filled and created repeatedly in two stages.

307 Table 1. Description and interpretation of the lithofacies documented in the outcrops.

| Code | Lithofacies description | Lithofacies geometry | Depositional process | Sedimentary environment | References |
|---|---|---|---|---|---|
| SGpm | coarse-grained sand with granules and mud intraclasts, occasional pebbles, massive to poorly-visible cross stratification, redeposited large mammal fossils | tabular and lenticular bodies with sharp base of complicated morphology and sharp upper boundary, 10–60 cm thick | rapid deposition from a waning flow with high concentration of coarse-grained sediment | decelerating flood in a river channel | Mulder and Alexander (2001); Carling and Leclair (2019); Ghinassi and Moody (2021) |
| St | trough cross-stratified medium to coarse sand, occasionally with fine gravel or mud intraclasts at the base | lenticular body with sharp concave upwards base and sharp upper boundary, 10–50 cm thick | sandy bedload channelized traction current | 3D dunes migrating in shallow parts of a channel and across bars | Allen (1982); Leclair and Bridge (2001); Reesink and Bridge (2011); Naqshband et al. (2017) |
| Stb | trough and planar cross-stratified units, foresets composed of various lithology (mud, intraclasts, fine- to coarse-grained sand, granules), strata commonly form internal angular contacts, foresets are occasionally formed by small scale trough cross-stratified sands and ripple cross-stratified sands with paleocurrent direction perpendicular to the foreset dip direction | lenticular body with sharp base of complicated morphology and sharp upper boundary, 20–60 cm thick | traction current of variable speed from ≤10 $cm \cdot s^{-1}$ to ~100 $cm \cdot s^{-1}$, flowing over an inclined surface | unit bar in a river channel, foresets formed by collapse of superimposed bedforms at the brink point (downstream accretion), or by bedforms migrating parallel to the bar surface strike (lateral accretion) | Miall (1985); Almeida et al. (2016); Reesink (2018) |
| Sl | medium- to coarse-grained sand with low angle inclined stratification, commonly lamination parallel to the basal accretionary surface, internal low-angle angular contacts of strata common | tabular bodies few cm thick with sharp boundaries | channelized traction current of upper plane bed flow to supercritical flow | upper plane beds to antidunes formed above bars in river channel during floods with increased flow speed | Bennett and Best (1997); Fielding (2006); Naqshband et al. (2017) |
| Sr | unidirectional ripples formed from medium- to fine-grained sand to silt | tabular body few cm thick with fluent boundaries or few cm thick lenticular body | shallow or slow traction current | ripples formed on a bar surface, in shallow channel or proximal overbank settings | Allen (1982); Baas (1999); Yawar and Schieber (2017) |

| | | | | | |
|---|---|---|---|---|---|
| Sm, FSm | massive medium to fine sand, containing muddy intraclasts, massive sandy mud | lenticular bodies 5-20 cm thick, with concave sharp erosional base and sharp upper boundary | rapid deposition from a waning flow | suddenly decelerating flood in abandoned shallow channel, in an oxbow lake or in a proximal floodplain | Mulder and Alexander (2001); Baas et al. (2016), Burns et al. (2017) |
| Fl | planar laminated mud, beige to light grey, lamination subhorizontal or parallel to the basal surface | continuous horizons few centimeters to 20 cm thick, with sharp lower and upper boundary | deposition from a slow traction current or from suspension | slack water deposition above a bar, in an oxbow lake or in a proximal floodplain | Aslan and Autin, (1999); Yawar and Schieber (2017) |
| Fm | massive mud, beige to light grey, locally lateral transition to intraclasts | continuous horizons and lenticular bodies few centimeters to 30 cm thick, with sharp lower and upper boundary | deposition from suspension of a high mud-concentrated waning flow | decelerating flood with high content of mud, oxbow lake or proximal floodplain | Toonen et al. (2011); Baas et al. (2016) |

## 5.2 Authigenic $^{10}Be/^{9}Be$ dating

The measured concentrations of nuclides, natural authigenic $^{10}Be/^{9}Be$ ratios and calculated ages are included in Table 2 and depicted in Fig. 3. The natural $^{10}Be/^{9}Be$ range is from $5.541 \times 10^{-10}$ to $20.175 \times 10^{-10}$. Ages reach values from 1.438 ± 0.048 Ma to 4.024 ± 0.111 Ma. The oldest ages, 4.024 ± 0.111 Ma and 3.802 ± 0.094 Ma, were yielded by samples NV-2-4 and NV-2-5 taken from the basal muddy horizon present below the base of the river terrace. Another group of ages is represented by the intraclast samples NV-1-4, NV-1-5 and NV-1-6, which attain 2.701 ± 0.093 Ma, 2.484 ± 0.096 Ma and 2.031 ± 0.076 Ma, respectively. The remaining seven samples originating from *in situ* layers reach ages in the range from 1.852 ± 0.060 Ma to 1.438 ± 0.048 Ma, except for an age of 2.303 ± 0.093 Ma for sample NV-1-1, which appears to be an outlier. The ages of *in situ* samples are not distributed systematically regarding either their vertical or lateral position.

Table 2. Concentrations of $^{9}$Be and $^{10}$Be, $^{10}$Be/$^{9}$Be ratios and calculated ages for the analyzed samples. Uncertainties are $\sigma_1$. Concentrations of $^{10}$Be are corrected to the $^{10}$Be/$^{9}$Be ratios of the two processing blanks reaching values of $7.75 \times 10^{-15}$, (sampling in 2016 and 2017) and $1.52 \times 10^{-14}$ (sampling in 2015).

| Sample ID | Year of sampling | Sample type | AMS $^{10}$Be/$^{9}$Be [$\times 10^{-12}$] | AMS uncertainty $^{10}$Be/$^{9}$Be [%] | $^{9}$Be measurement | Natural $^{9}$Be [atom g $\times 10^{16}$] | $^{9}$Be standard deviation [%] | Natural $^{10}$Be [atom g $\times 10^{7}$] | Uncertainty $^{10}$Be [atom · g $\times 10^{7}$] | Natural $^{10}$Be/$^{9}$Be [$\times 10^{-10}$] | Uncertainty $^{10}$Be/$^{9}$Be [$\times 10^{-10}$] | Authigenic $^{10}$Be/$^{9}$Be depositional age [Ma] |
|---|---|---|---|---|---|---|---|---|---|---|---|---|
| NV-1-1 | 2015 | in situ layer | 1,545 | 3,503 | AAS | 2,391 | 2,941 | 3,132 | 0,110 | 13,098 | 0,528 | 2,303 ± 0,093 |
| NV-1-2 | 2015 | in situ layer | 3,332 | 2,555 | AAS | 4,122 | 0,959 | 6,764 | 0,173 | 16,411 | 0,533 | 1,852 ± 0,060 |
| NV-1-3 | 2015 | in situ layer | 3,041 | 2,674 | AAS | 3,046 | 1,398 | 6,145 | 0,164 | 20,175 | 0,674 | 1,438 ± 0,048 |
| NV-1-4 | 2015 | intraclast | 2,936 | 3,171 | AAS | 3,961 | 1,429 | 5,942 | 0,188 | 15,002 | 0,562 | 2,031 ± 0,076 |
| NV-1-5 | 2015 | intraclast | 2,736 | 3,323 | AAS | 4,622 | 1,441 | 5,529 | 0,184 | 11,963 | 0,464 | 2,484 ± 0,096 |
| NV-1-6 | 2015 | intraclast | 2,503 | 2,800 | AAS | 4,712 | 2,931 | 5,057 | 0,142 | 10,733 | 0,369 | 2,701 ± 0,093 |
| NV-2-1 | 2016 | in situ layer | 3,941 | 1,312 | ICP-MS | 6,252 | 5,438 | 12,128 | 0,159 | 19,397 | 0,464 | 1,517 ± 0,036 |
| NV-2-2 | 2016 | in situ layer | 5,001 | 1,392 | ICP-MS | 7,667 | 4,980 | 15,371 | 0,214 | 20,049 | 0,489 | 1,451 ± 0,035 |
| NV-2-3 | 2016 | in situ layer | 3,566 | 1,336 | ICP-MS | 5,944 | 5,074 | 10,882 | 0,145 | 18,306 | 0,440 | 1,633 ± 0,039 |
| NV-2-4 | 2016 | basal muds | 1,739 | 1,912 | ICP-MS | 9,516 | 3,376 | 5,272 | 0,101 | 5,541 | 0,153 | 4,024 ± 0,111 |
| NV-2-5 | 2016 | basal muds | 2,183 | 1,435 | ICP-MS | 10,785 | 1,968 | 6,679 | 0,096 | 6,193 | 0,152 | 3,802 ± 0,094 |
| NV-3-1 | 2017 | in situ layer | 3,349 | 1,335 | ICP-MS | 5,896 | 2,692 | 10,261 | 0,137 | 17,403 | 0,419 | 1,734 ± 0,042 |
| NV-3-2 | 2017 | in situ layer | 3,368 | 1,332 | ICP-MS | 6,084 | 4,145 | 10,270 | 0,137 | 16,881 | 0,406 | 1,795 ± 0,043 |

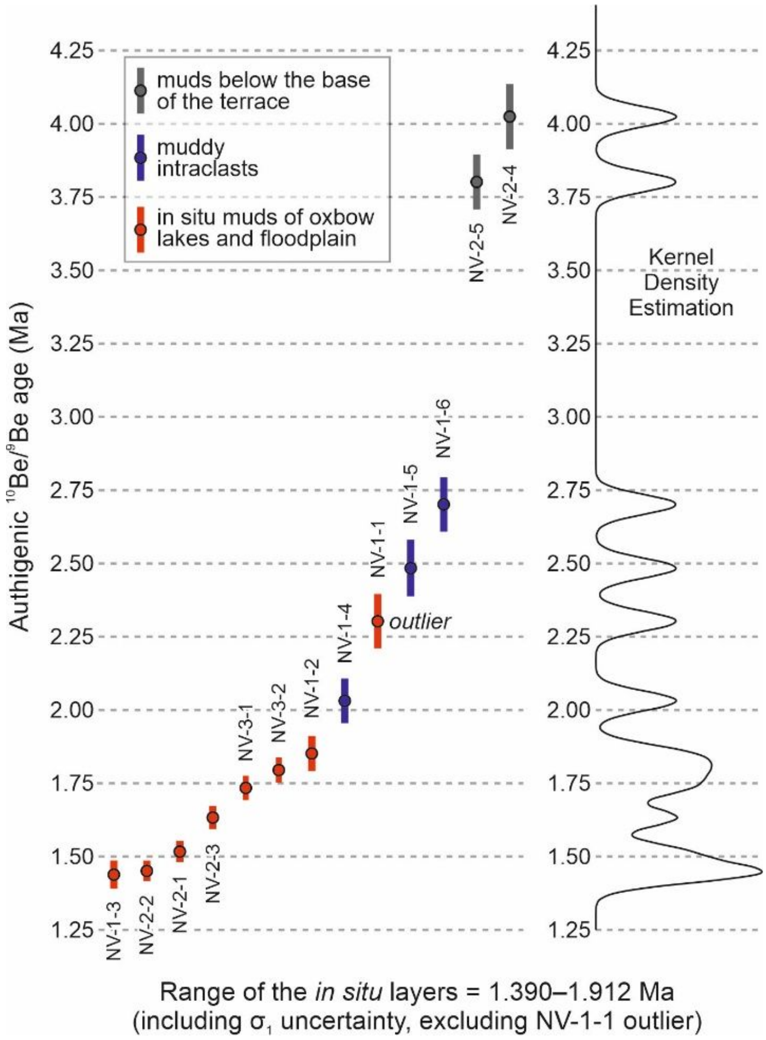


Fig. 3. Distribution of the authigenic $^{10}$Be/$^{9}$Be ages depicted in ascending order of the values and Kernel Density Estimation, obtained using the KDX application (Spencer et al., 2017). Depicted uncertainties are $\sigma_1$.

# 6. Sedimentological interpretations

## 6.1 Depositional processes

The lithofacies SGpm was deposited during waning of a surge-type flow with a high concentration of gravelly and sandy sediment, which led to a low degree of effectivity of turbulence, in turn causing a low degree of sorting and only a weak development of stratification, which is even missing locally (Mulder and Alexander, 2001; Cartigny et al., 2013;

Carling and Leclair, 2019; Ghinassi and Moody, 2021) (Figs. 4E, 5C). The base of SGpm units is usually complicated and erosional, and SGpm commonly contains intraclasts of the underlying cohesive strata (Fig. 5C). Trough cross-stratified sands were deposited as 3D dunes by traction currents (Allen, 1982; Leclair and Bridge, 2001; Reesink and Bridge, 2011; Naqshband et al., 2017) (Figs. 4D, 6, 9).

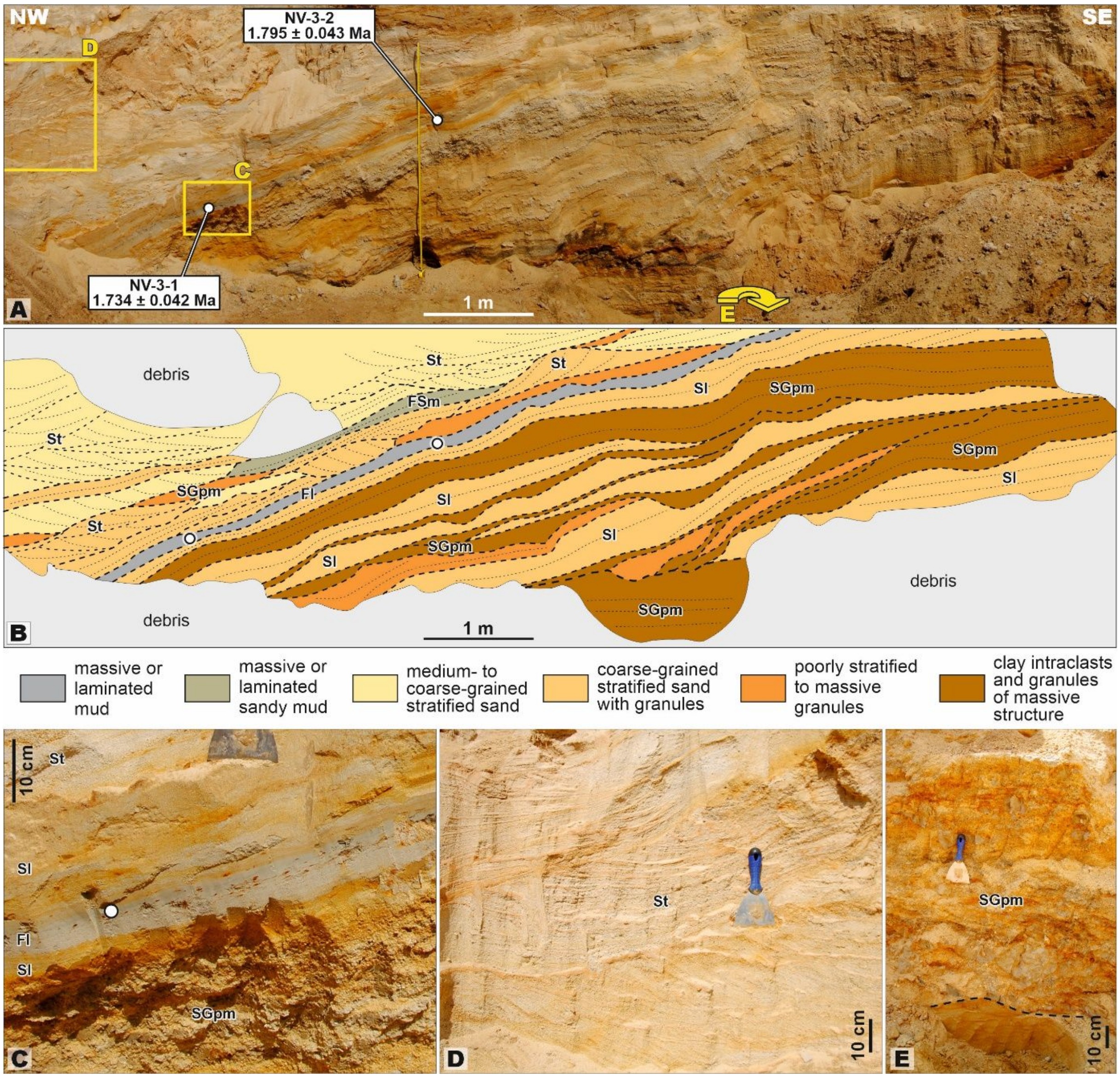


Fig. 4. Outcrop wall oriented in a NW-SE direction and sampled for authigenic $^{10}Be/^{9}Be$ (white dots). (A,B) Inclined strata forming ca 2.5 m thick bar with variable lithology, implying changes in the current speed and sediment concentration. Orientation of trough-cross strata indicate lateral accretion origin of the bar. (C)

Laminated mud strata sampled for the dating. (D) Trough cross-stratified strata. (E) Poorly sorted gravelly sand with intraclasts. For location of the outcrop, see Fig. 1D,E.

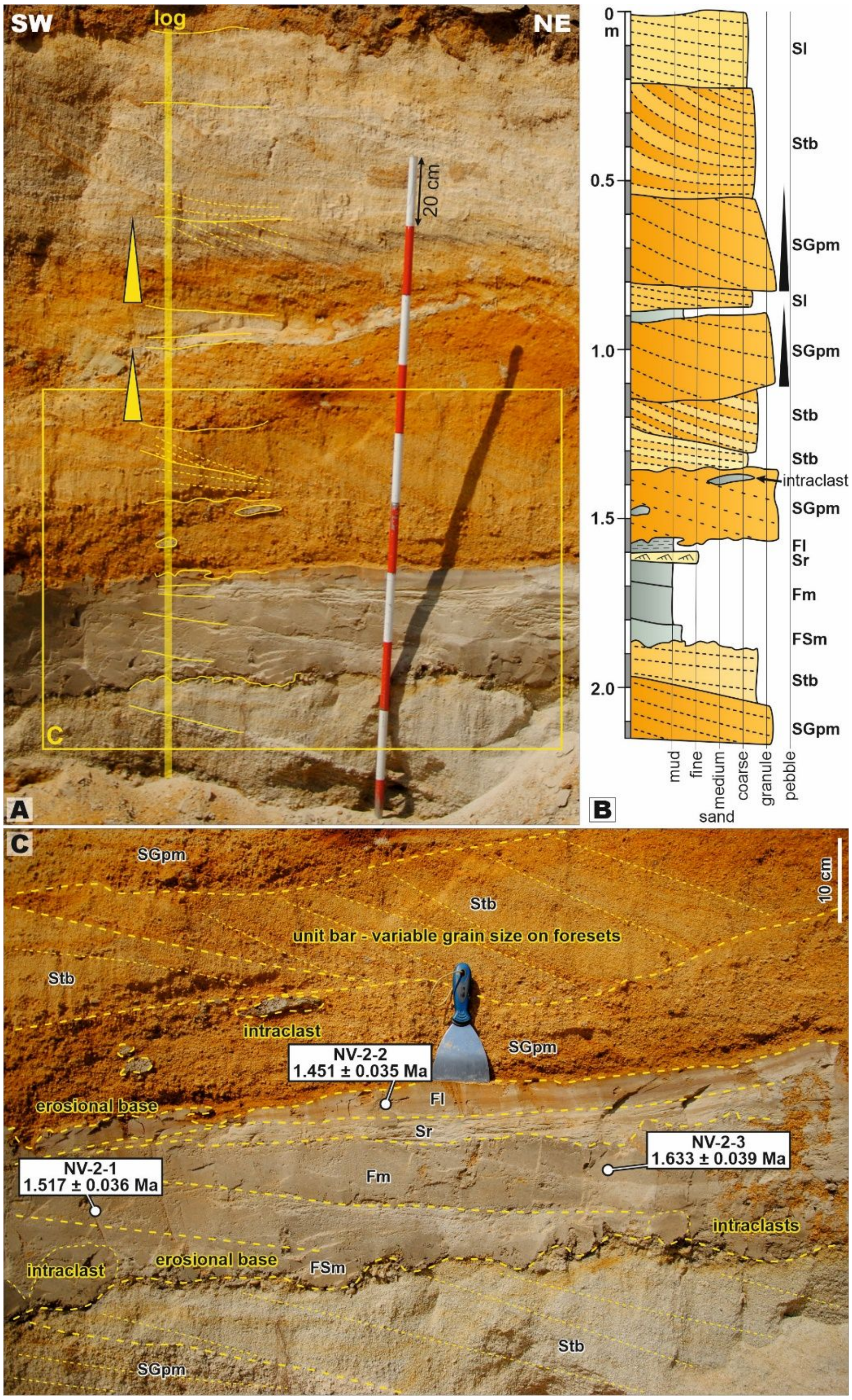

Fig. 5. Outcrop wall oriented in a SW-NE direction and sampled for authigenic $^{10}Be/^{9}Be$ (white dots). Note the muddy horizon, up to 30 cm thick, of a shallow oxbow lake fill and angular contacts within the unit bar of the Stb lithofacies on (C). For location of the outcrop, see Fig. 1D,E.

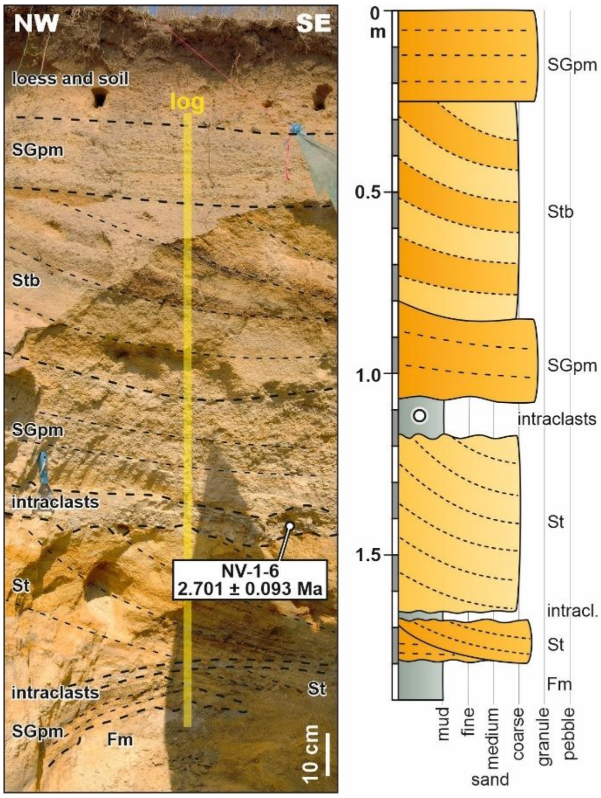


Fig. 6. Outcrop wall oriented NW-SE, sampled for authigenic $^{10}Be/^{9}Be$ (white dot). The sample originates from a layer of accumulated intraclasts. For location of the outcrop, see Fig. 1D,E.

The Stb facies, consisting of inclined strata of variable lithology from gravel to mud, and with the presence of trough or ripple cross-strata within the inclined accretion units, represents fluvial bars formed in a channel (Miall, 2006; Almeida et al., 2016; Reesink, 2018; Herbert et al., 2020). The great degree of variability in grain size indicates significant changes in the flow speed, while the internal angular contacts of the accretion units resulted from erosion preceding reactivation of a bar. From the geometry of the accretion, it is possible to distinguish unit bars accreted downstream (Fig. 7A, B) (Reesink, 2018), and laterally accreted point bars (Fig. 7C,

D) in which a paleocurrent depositing superimposed dunes was oriented perpendicular to the direction of accretion (Almeida et al., 2016).

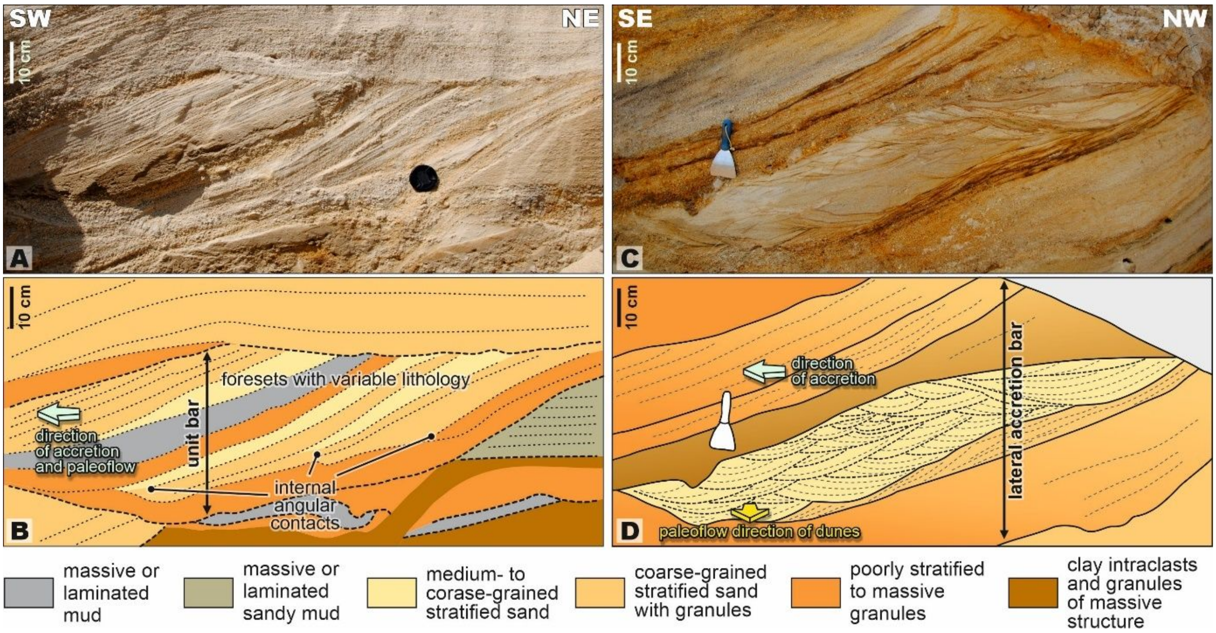


Fig. 7. Examples of a unit bar (A, B) and lateral accretion bar (C, D). (A, B). Note the variable lithology and internal angular contacts in the unit bar, indicating the variable transport capacity of a flow. (C, D). Note the perpendicular direction of bar accretion and of general paleoflow orientation indicated by trough cross-stratifications in the lateral accretion. For location of the outcrop, see Fig. 1D, E.

Medium- to coarse-grained sands showing subhorizontal or slightly inclined stratification or stratification parallel to an accretion surface of a bar are included in the Sl lithofacies (Figs. 4, 5, 8). This is interpreted as forming the upper stage plane beds or antidunes deposited by a transitional or supercritical flow (Bennett and Best, 1997; Fielding, 2006; Naqshband et al., 2017). Silty, fine- to medium-grained sandy ripple cross-strata were deposited as a ripple bedform by a unidirectional traction current with a low speed and/or shallow depth (Allen, 1982; Baas, 1999; Yawar and Schieber, 2017) (Fig. 5C). On the other hand, bodies of massive fine- to medium-grained sand (Sm) or sandy mud with intraclasts (FSm) accumulated from a waning surge-type flow with a high concentration of sediment, possibly in an abandoned channel, in an oxbow lake or in a proximal floodplain, depending on whether the unit forms a lens in a depression or a more continuous horizon (Mulder and Alexander, 2001; Baas et al., 2016) (Fig. 5C).

Planar laminated mud of the Fl lithofacies is interpreted as a deposit occasioned by a slow traction current (<0.25 $m \cdot s^{-1}$) or of suspension fallout in slack water conditions (Aslan and Autin, 1999; Yawar and Schieber, 2017) (Figs. 4C, 5, 9C, D). It was formed above a bar, in an oxbow lake or in a proximal floodplain, depending on the relation to the geometry of underlying strata. The last observed lithofacies consisting of massive mud (Fm) is frequently associated with intraclasts and its appearance indicates rapid deposition from a waning flow with a high concentration of mud, likely representing a flood decelerating in an oxbow lake or in a proximal floodplain (Toonen et al., 2012; Baas et al., 2016).

## 6.2 Deformations

The large-scale involution in Fig. 8 was formed during the deposition of the studied succession, since it is overlain by undeformed strata which accumulated in a river channel (the Stb, St and Sl facies). The deformed horizon also comprises river channel deposits, as indicated by the remnants of trough cross-stratification within the deformed beds. The preservation of primary bedding and the geometry of involution imply a plastic deformation by a relatively continuous process, and this does not imply seismic shock as the trigger. The sediment was likely under the influence of a nearby stream, which deposited the overlying strata later, and hence the strata were saturated with water. Accordingly, changes in rheology during freeze-thaw cycles and the related loss of frictional strength could be considered part of the formation process of the involution (van Vliet-Lanoë et al., 2004; Vandenberghe, 2013). The decimeter-scale graben-like collapses (Fig. 8G) are likely associated with local extension due to the frost contraction of the deformed unit. The evidence for the deformation of the studied strata by cryoturbation is supported by the frequent presence of sand wedges (Fig. 9A). The wedges exhibit features of frost contraction, the forming of an open crack, which is then filled by the overlying sediment (Murton et al., 2000). Flame structures and plastic deformation of the muds located below the base of river terrace (Fig. 10) might also be explained by plastic deformation due to differential loading by freeze-thaw cycles (Horváth et al., 2005; Vandenberghe, 2013). The cryogenic deformation of the basal muddy horizon indicates its surface exposure during glacial. All comparable structures of cryogenic deformation are present with some frequency in the region (Horváth et al., 2005; Ruszkiczay-Rüdiger and Kern, 2016).

The deformation most infrequently present is the symmetrical downwards bending of strata with decreasing intensity downwards (Fig. 9B). These marks are geometrically similar to the tracks of large mammals (Nadon et al., 2001; Fornós et al., 2002; Milán et al., 2015). Their isolated presence in the outcrops, however, in combination with a relatively deep reach of the deformation and the absence of some mixing of the uppermost strata due to the impact of a foot makes this interpretation problematic. Another explanation might be the deformation of the sediment by a growing tree root (do Nascimento et al., 2019). Remnants of limonitized wood are common in the SGpm facies (Vlačiky et al., 2017). The burrows with simple morphology filled by sediment derived from overlying layers (Fig. 9C) resemble crayfish burrows, which are common in comparable riverine sedimentary environments (Smith et al., 2008; Abouessa et al., 2015; Buatois et al., 2020). Another, less likely explanation might be formation by dwelling of small mammals (Gobetz and Martin, 2006; Hembree and Hasiotis, 2008).

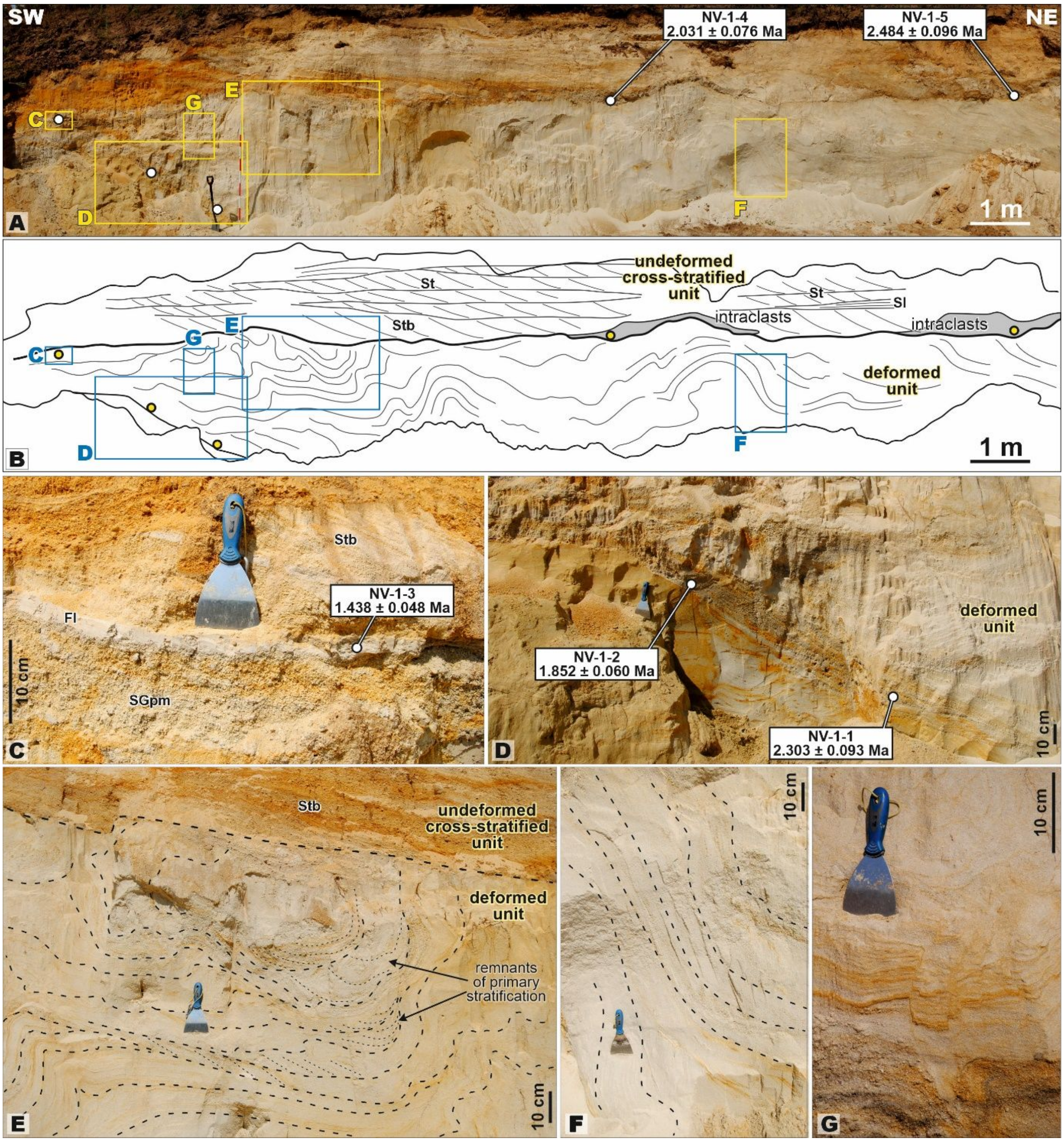


Fig. 8. Outcrop wall oriented SW-NE, sampled for authigenic $^{10}Be/^{9}Be$ (white dots). (A, B) the lower unit exhibits intense deformation of the whole, ca. 2.5 m thickness, while the original structures of the upper unit are preserved. Orientation of trough-cross strata indicate lateral accretion origin of the bar. (C, D) Laminated mud strata sampled for dating. (E) Detail of the deformation with preserved remnants of the original trough cross-stratification. (F) Detail of the deformation with almost vertically oriented strata. (G) Small-scale brittle collapse structure within the lower deformed unit. For location of the outcrop, see Fig. 1D, E.

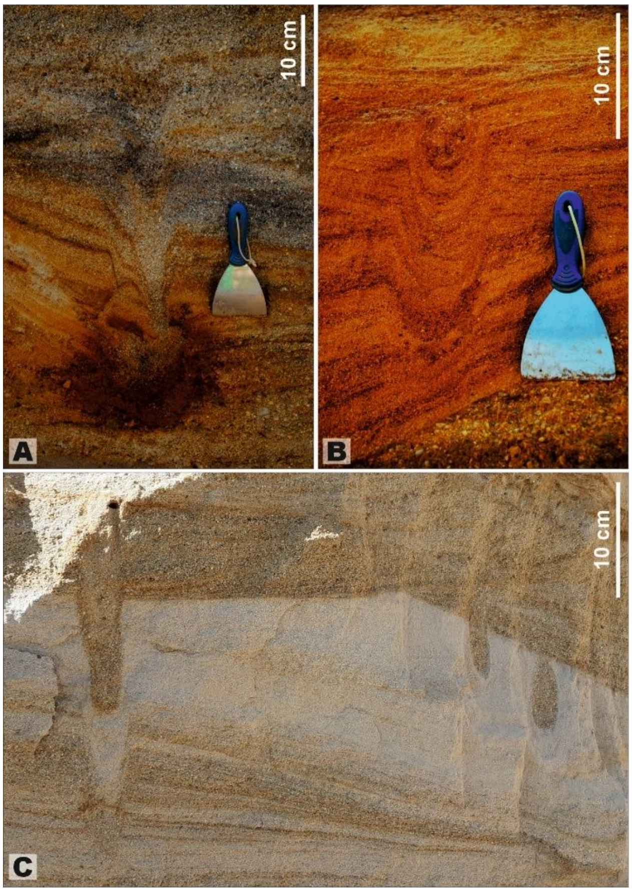


Fig. 9. Examples of deformations observable at the Nová Vieska site. (A) Sand wedge formed by cryoturbation. (B) A mark, possibly the track of a large mammal, or due to the growth of a tree root. (C) Structures possibly formed as the burrows of crayfish or small mammals.

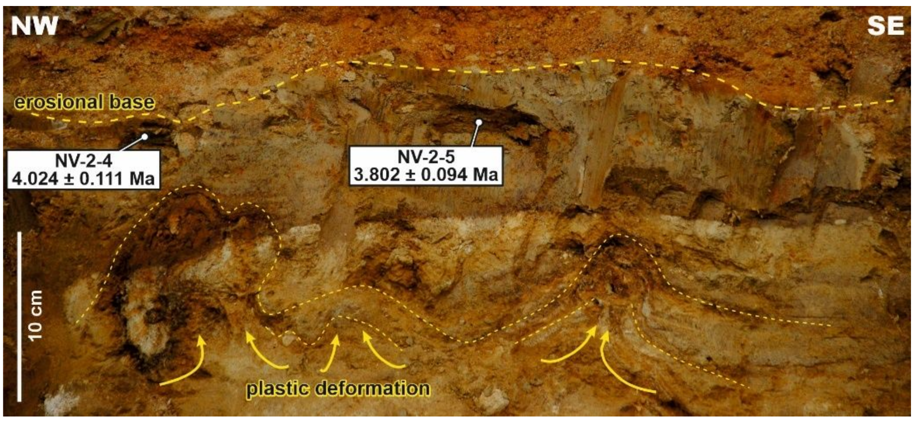


Fig. 10. Basal muds appearing below the base of the river terrace. Note the flame structure plastic deformations. For location of the outcrop, see Fig. 1D, E.

## 6.3 Sedimentary environment

The thickness of the bars deposited within fluvial channels varies considerably, from 0.4 m (Fig. 7) to the highest observed thickness of 2.5 m, represented by the inclined sedimentary unit in Fig. 4A, B. The thickness of a bar is generally equal to the depth of the channel, hence, the succession here was likely to have accumulated in a network of channels of various depths (Bridge and Tye, 2000). Several facts point to the sedimentary environment of a wandering river: the presence of both types of unit bars, those formed by downstream and lateral accretion; the low accommodation to sediment supply ratio indicated by low preservation of muddy overbank and oxbow lake facies; and the indications of variable channel sizes (Forbes, 1983; Miall, 2006; Long and Lowey, 2011) (Fig. 11A). This interpretation then agrees with previous sedimentological research performed at the site by Vlačiky et al. (2008). The river regime was characterized by deposition from perennial flow with significant proportion of surge-type flows, indicating the presence of some discharge variability, potentially linked to climatic causes (Fielding et al., 2018; Alexander et al., 2020; Hansford et al., 2020; Herbert et al., 2020).

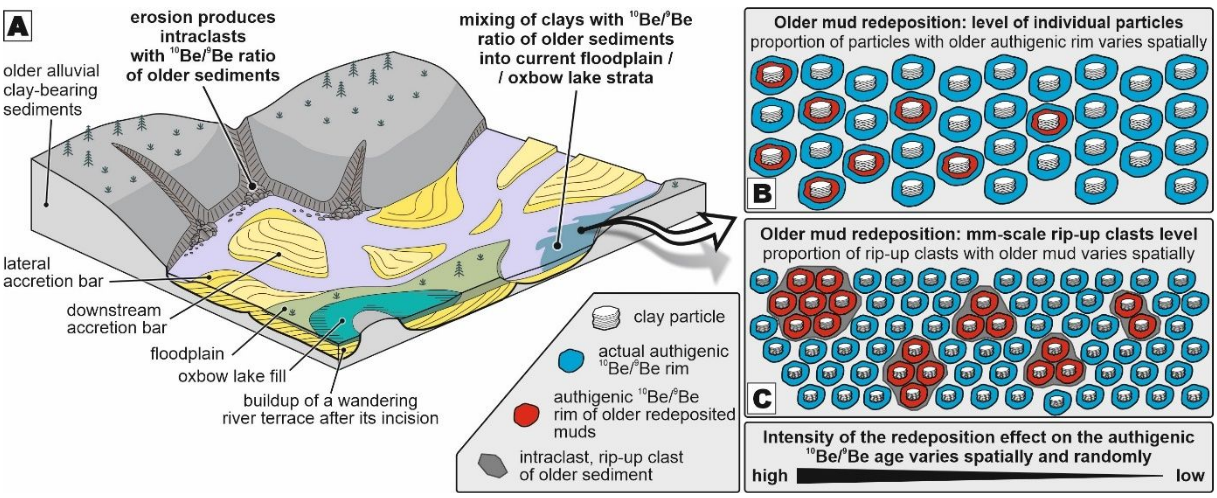


Fig. 11A. Block-diagram showing a wandering river facies model as a sedimentological interpretation of the succession under consideration here. The model implements the incision and redeposition of underlying alluvial succession as a factor affecting the authigenic $^{10}$Be/$^{9}$Be dating. Facies model modified from Miall

(2006). B. Schematic hypothesis of redeposition of older mud into younger sediment by mixing at the level of individual particles. Two authigenic rims are formed around the redeposited particles, with inner one preserving the $^{10}Be/^{9}Be$ ratio of the older bed. C. Schematic hypothesis of redeposition of older mud into younger sediment at the level of millimeter-scale intraclasts/rip-up clasts. The redeposition effect on the measured $^{10}Be/^{9}Be$ ratio of a sample may be expected to vary spatially, driven by the stochastic character of random distribution of the redeposition intensity in an incising river paleoenvironment.

Considering the geomorphological position of the studied accumulation as a river terrace surrounded by hills composed of older sediments (Fig. 1C), several features indicate the incision and denudation of the older alluvial deposits and their redeposition as an important aspect of sedimentary environment of the Nová Vieska succession: the timing of the sedimentation during the basin inversion; the base-level fall recorded in the river terrace staircase formation; and the abundant occurrence of clay intraclasts composed of floodplain facies (Fig. 11).

# 7. Depositional age and redeposition as a factor affecting authigenic $^{10}Be/^{9}Be$ dating

The authigenic ages show a relatively large time span; however, separating them into three groups allows the determination of a narrower depositional age interval for the Nová Vieska succession. The two ages 4.024 ± 0.111 Ma and 3.802 ± 0.094 Ma obtained from the muds below the base of the river terrace imply their affinity to the Pliocene Kolárovo Formation. Thus, this sedimentary formation, which is related to the base-level rise and aggradation in the basin, was preserved, at least locally, after the incision active after ~3 Ma, and it is not always the Volkovce Formation which appears below the river terraces in the area.

Upon analysis, the intraclasts yielded ages ~0.2–1.4 Myr higher than the *in situ* layers, after excluding sample NV-1-1, which was considered an outlier. The depositional model in Fig. 11A allows this difference to be attributed to the redeposition of older sediment during incision. The mixing of the older muddy sediment into younger strata on the level of individual sediment particles would result in the formation of two authigenic rims around a particle, one older, with a $^{10}$Be/$^{9}$Be ratio pertaining to the redeposited sediment, and the second outer one formed at the time of deposition, with the $^{10}$Be/$^{9}$Be ratio of the incising river waters (Fig. 11B). Since it is not possible to separate several authigenic rims during extraction, this effect would result in an apparently older authigenic $^{10}$Be/$^{9}$Be age. It is assumed that the older authigenic phase was not exposed to pH<4 and therefore remains intact despite the repeated dispersion of sedimentary particles in a water column (Willenbring and von Blanckenburg, 2010). Another possible path for the redeposition of older mud into younger sediment is on the level of millimeter-size rip-up clasts, scattered in the sediment with the then-current $^{10}$Be/$^{9}$Be ratio (Fig. 11C).

The ratio of both rims forming the resulting isotopic ratio of a sample under analysis should be scaled to how strong the input of older redeposited mud to a specific bed is, regardless of whether it is achieved at the level of individual particles or rip-up clasts. The input of older mud mixed will vary randomly across a sedimentary environment, especially in such a topographically differentiated environment as a wandering river with channels of various depths and hierarchies, and with flows taking place across a wide scale of speed, turbulence, and transport capacity. Hence, taken together these effects should widen the range of authigenic $^{10}$Be/$^{9}$Be ratios and ages within a single succession, as has been observed in the set of samples in this study.

The erosion of muddy strata, the production of rip-up clasts and the mixing of mud by traction currents have all been observed in flume experiments (Schieber et al., 2010; Noack et al., 2015; Van Rijn, 2020). Even if composed of unconsolidated and non-lithified mud, the intraclasts might be prone to being transported over considerable distances (Schieber, 2016). The muddy rip-up clasts attain a sub-millimeter to centimeter scale, and visual recognition of their presence in a bed might not be straightforward in the field. Processes of mud redeposition as rip-up intraclasts or a mixture are a common feature observed in fluvial environments (Müller et al., 2004; Li et al., 2017; Perkey et al., 2020; Li et al., 2021). Flows with high erosion potential took place during the deposition of the succession in the present study (Fig. 11A).

The effect described above of the mixing of mud with the preserved older authigenic $^{10}Be/^{9}Be$ signal may be considered a reasonable hypothesis for the explanation of the wide range of authigenic $^{10}Be/^{9}Be$ ages of the *in situ* layers, a range broad enough that they rarely overlap within $\sigma_1$ uncertainties. The analytical uncertainties therefore cannot mirror the paleoenvironmental variability caused by the redeposition and mixing. Thus, it may be assumed that the most robust approach in the determination of the depositional age of the outcrop is to use the full range of the *in situ* layers ages within error bars, an approach which yields a figure of 1.390–1.912 Ma.

The depositional age established is not in agreement with the age range ~3.6–2.2 Ma indicated by the biostratigraphy of large mammal fossils from the succession. Nevertheless, all fossils are present as clasts in the channel-fill facies, and hence must have been redeposited. The dated intraclasts do have ages in accordance with the mammal biostratigraphic age range, pointing to the possibility of the same source of material during redeposition.

The hypothesis of the redeposition of older sediment as a factor affecting the authigenic $^{10}Be/^{9}Be$ dating requires further verification. A validation of the hypothesis by petrographic or geochemical proxies remains problematic, as the floodplain muddy facies of the redeposited Volkovce and Kolárovo fms. as well as the Quaternary sediments were deposited by comparable processes and with a similar provenance (Šujan et al., 2018; Šujan et al., 2020). Whether different climatic conditions would allow the tracing of the effect described here in the muddy layers remains an open question. The mixing of older mud as a cause of the apparently older ages derived from $^{10}Be/^{9}Be$ dating was documented by the redeposition of microfossils in the turbiditic succession deposited on the basin floor of Lake Pannon in the Danube Basin (Šujan et al., 2016). This approach is not, however, suitable for terrestrial facies.

The extensive occurrence of cryogenic deformations and their burial point to sedimentation taking place during glacials (Vandenberghe, 2013). The evolution of mean annual temperatures (MAT) in the period of ~2.58–1.80 Ma in Central Europe (Kahlke et al., 2011; Kovács et al., 2015; Martinetto et al., 2015; Teodoridis et al., 2017) contain values which are not cool enough to produce the observed deformations (Ruszkiczay-Rüdiger and Kern, 2016). It is suggested that glaciation in Europe only took place after 1.8 Ma, and its more significant extension in the Alps and Carpathians even after 1.2–0.9 Ma (Muttoni et al., 2003; Van Husen, 2004; Gibbard and Lewin, 2009; Knudsen et al., 2020). Hence, the extensive presence of cryogenic deformations in the Nová Vieska succession favors the age range of 1.390–1.912 Ma established in this study using authigenic $^{10}Be/^{9}Be$ dating.

# 8. Conclusions

This study aimed to investigate suitability of incising river deposits formed under conditions of low accommodation and high sediment supply for dating using the authigenic $^{10}Be/^{9}Be$ method. The Nová Vieska river terrace succession, located in the eastern Danube Basin, comprises facies from a wandering river, mostly unit bars accreted downstream and lateral accretion bars. Facies analysis implied a high degree variability in flow speed, turbulence and sediment concentration, and these, in turn, resulted in a wide range of lithologies, from gravelly sands to *in situ* muddy strata of proximal floodplain and oxbow lake deposits forming a minor part of the succession. Redeposition of mud from older eroded strata during incision of the river, related to the ongoing inversion of the basin, was an important feature of the sedimentary environment, as is evidenced by the widespread occurrence of mud intraclasts.

Authigenic $^{10}Be/^{9}Be$ dating yielded ages which may then be attributed to three groups of samples: (1) two ages of 4.024 ± 0.111 Ma and 3.802 ± 0.094 Ma from the strata below the base of the river terrace; (2) three ages of 2.701 ± 0.093 Ma, 2.484 ± 0.096 Ma and 2.031 ± 0.076 Ma obtained from intraclasts of the redeposited mud; and (3) six ages in the range of 1.852 ± 0.060 Ma to 1.438 ± 0.048 Ma yielded by analysis of *in situ* muddy strata, with one outlier reaching an age of 2.303 ± 0.093 Ma.

The distribution pattern of authigenic $^{10}Be/^{9}Be$ ages may be interpreted as the result of the redeposition of older mud derived from the incised substrate, which consists predominantly of muddy alluvial sediments. It is proposed that the hypothesis of redeposition as a factor affecting authigenic $^{10}Be/^{9}Be$ dating may be observed at three scales: (1) redeposition of decimeter-scale intraclasts with the original age of the older substrate preserved, (2) redeposition of millimeter-scale rip-up clasts preserving the $^{10}Be/^{9}Be$ ratio of the older substrate, and which are mixed into younger strata in random proportions, and (3) redeposition at the scale of individual particles, leading to the formation of two authigenic rims, the inner one preserving the older $^{10}Be/^{9}Be$ ratio, and the outer one representing the $^{10}Be/^{9}Be$ ratio current during deposition. The proportion of particles with preserved older authigenic $^{10}Be/^{9}Be$ rims would also vary randomly across the depositional environment. The stochastic spatial variation of the admixture of older mud particles or rip-up clasts is considered to be the reason for the wide range of the ages obtained from *in situ* muddy layers. Taking into account all the assumptions mentioned here, the full range of the authigenic $^{10}Be/^{9}Be$ ages yielded by the *in situ* mud samples falls between 1.390 and 1.912 Ma (within the margin of uncertainty), and it is this which is proposed as the age of deposition of the succession.

The established age range differs from the interval ~3.6–2.2 Ma provided by the large mammal biostratigraphy; these fossils, however, accumulated as clasts and likely underwent redeposition from the same source as the similarly aged intraclasts. The extensive occurrence of cryogenic deformations also favors the age range provided by the authigenic $^{10}Be/^{9}Be$ dating, since the climatic conditions needed for such deformations to take place appeared in Central Europe only at this later time.

The hypothesis of mud redeposition during incision of a river as an effect affecting their authigenic $^{10}Be/^{9}Be$ dating needs further investigation and verification. The discovery of this effect serves to emphasize that conditions of high accommodation to sediment supply ratio are much more favorable for the application of the method (e.g., Šujan et al., 2020), since such conditions minimize the redeposition of mud with various authigenic $^{10}Be/^{9}Be$ ratios. The potential influence of the redeposition effect on the authigenic $^{10}Be/^{9}Be$ dating method should be considered in future studies of continental sedimentary successions deposited in conditions of low accommodation rates.

## Acknowledgements

The study was supported by the Slovak Research and Development Agency (APVV) under contract Nos. APVV-16-0121 and APVV-20-0120. ASTER AMS national facility (CEREGE, Aix-en-Provence) is supported by the INSU/CNRS, the ANR through the “Projets thématiques d'excellence” program for the “Equipements d'excellence” ASTER-CEREGE action and IRD. Zsófia Ruszkiczay-Rüdiger is thanked for her kind advice during interpretation of cryogenic deformations and dating results. The free availability of the Lidar DEM data from the Geodesy, Cartography and Cadastre Authority of the Slovak Republic is acknowledged with gratitude. Paul Thatcher is thanked for his efforts made during the language correction.

# References


Abouessa, A., Duringer, P., Schuster, M., Pelletier, J., 2015. Crayfish fossil burrows, a key tool for identification of terrestrial environments in tide-dominated sequence, Upper Eocene, Sirt Basin, Libya. Journal of African Earth Sciences 111, 335-348.

Alexander, J., Herbert, C.M., Fielding, C.R., Amos, K.J., 2020. Controls on channel deposits of highly variable rivers: Comparing hydrology and event deposits in the Burdekin River, Australia. Sedimentology 67, 2721-2746.

Allen, J.R.L., 1982. Sedimentary Structures: Their Character and Physical Basis. Elsevier, Amsterdam.

Almeida, R.P., Freitas, B.T., Turra, B.B., Figueiredo, F.T., Marconato, A., Janikian, L., 2016. Reconstructing fluvial bar surfaces from compound cross-strata and the interpretation of bar accretion direction in large river deposits. Sedimentology 63, 609-628.

Aslan, A., Autin, W.J., 1999. Evolution of the Holocene Mississippi River floodplain, Ferriday, Louisiana: Insights on the origin of fine-grained floodplains. Journal of Sedimentary Research 69, 800-815.

Baas, J.H., 1999. An empirical model for the development and equilibrium morphology of current ripples in fine sand. Sedimentology 46, 123-138.

Baas, J.H., Best, J.L., Peakall, J., 2016. Predicting bedforms and primary current stratification in cohesive mixtures of mud and sand. Journal of the Geological Society 173, 12-45.

Bennett, S., Best, J., 1997. Bed-load motion at high shear stress: Dune washout and plane-bed flow. Journal of Hydraulic Engineering 123, 375-377.

Bernhardt, A., Oelze, M., Bouchez, J., von Blanckenburg, F., Mohtadi, M., Christl, M., Wittmann, H., 2020. $^{10}$Be/$^{9}$Be Ratios Reveal Marine Authigenic Clay Formation. Geophysical Research Letters 47.

Bourlès, D., Raisbeck, G.M., Yiou, F., 1989. $^{10}$Be and $^{9}$Be in marine sediments and their potential for dating. Geochimica et Cosmochimica Acta 53, 443-452.

Bridge, J.S., Tye, R.S., 2000. Interpreting the dimensions of ancient fluvial channel bars, channels, and channel belts from wireline-logs and cores. Aapg Bulletin 84, 1205-1228.

Brown, E.T., Edmond, J.M., Raisbeck, G.M., Bourlès, D.L., Yiou, F., Measures, C.I., 1992. Beryllium isotope geochemistry in tropical river basins. Geochimica et Cosmochimica Acta 56, 1607-1624.

Buatois, L.A., Wetzel, A., Mángano, M.G., 2020. Trace-fossil suites and composite ichnofabrics from meandering fluvial systems: The Oligocene Lower Freshwater Molasse of Switzerland. Palaeogeography, Palaeoclimatology, Palaeoecology 558, 109944.

Burchfiel, B., Nakov, R., Tzankov, T., Royden, L., Bozkurt, E., Winchester, J., Piper, J., 2000. Tectonics and Magmatism in Turkey and the Surrounding Area. Geological Society of London Special Publication 173, 325-352.

Carcaillet, J., Bourlès, D.L., Thouveny, N., Arnold, M., 2004. A high resolution authigenic $^{10}$Be/$^{9}$Be record of geomagnetic moment variations over the last 300 ka from sedimentary cores of the Portuguese margin. Earth and Planetary Science Letters 219, 397-412.

Carling, P.A., Leclair, S.F., 2019. Alluvial stratification styles in a large, flash-flood influenced dryland river: The Luni River, Thar Desert, north-west India. Sedimentology 66, 102-128.

Cartigny, M.J.B., Eggenhuisen, J.T., Hansen, E.W.M., Postma, G., 2013. Concentration-dependent flow stratification in experimental high-density turbidity currents and their relevance to turbidite facies models. Journal of Sedimentary Research 83, 1046-1064.

do Nascimento, D.L., Batezelli, A., Ladeira, F.S.B., 2019. The paleoecological and paleoenvironmental importance of root traces: Plant distribution and topographic significance of root patterns in Upper Cretaceous paleosols. CATENA 172, 789-806.

Dunai, T., 2010. Cosmogenic Nuclides. Principles, Concepts and Applications in the Earth Surface Sciences. Cambridge University Press.

Fielding, C.R., 2006. Upper flow regime sheets, lenses and scour fills: Extending the range of architectural elements for fluvial sediment bodies. Sedimentary Geology 190, 227-240.

Fielding, C.R., Alexander, J., Allen, J.P., 2018. The role of discharge variability in the formation and preservation of alluvial sediment bodies. Sedimentary Geology 365, 1-20.

Forbes, D., 1983. Morphology and sedimentology of a sinuous gravel-bed channel system: lower Babbage River, Yukon coastal plain, Canada, Modern and ancient fluvial systems. Inter. Assoc. Sedim. Spec. Publ., 6, pp. 195-206.

Fornós, J.J., Bromley, R.G., Clemmensen, L.B., Rodríguez-Perea, A., 2002. Tracks and trackways of Myotragus balearicus Bate (Artiodactyla, Caprinae) in Pleistocene aeolianites from Mallorca (Balearic Islands, Western Mediterranean). Palaeogeography, Palaeoclimatology, Palaeoecology 180, 277-313.

Ghinassi, M., Moody, J., 2021. Reconstruction of an extreme flood hydrograph and morphodynamics of a meander bend in a high-peak discharge variability river (Powder River, USA). Sedimentology 68, 3549-3576.

Gibbard, P.L., Lewin, J., 2009. River incision and terrace formation in the Late Cenozoic of Europe. Tectonophysics 474, 41-55.

Gobetz, K.E., Martin, L.D., 2006. Burrows of a gopher-like rodent, possibly Gregorymys (Geomyoidea: Geomyidae: Entoptychtinae), from the early Miocene Harrison Formation, Nebraska. Palaeogeography, Palaeoclimatology, Palaeoecology 237, 305-314.

Graham, I.J., Ditchburn, R.G., Whitehead, N.E., 2001. Be isotope analysis of a 0–500 ka loess–paleosol sequence from Rangitatau East, New Zealand. Quaternary International 76–77, 29-42.

Graly, J.A., Bierman, P.R., Reusser, L.J., Pavich, M.J., 2010. Meteoric $^{10}Be$ in soil profiles: a global meta-analysis. Geochimica et Cosmochimica Acta 74, 6814-6829.

Hansford, M.R., Plink-Björklund, P., Jones, E.R., 2020. Global quantitative analyses of river discharge variability and hydrograph shape with respect to climate types. Earth-Science Reviews 200, 102977.

Harčár, J., Schmidt, Z., 1965. Kvartér v okolí Strekova na Hronskej pahorkatine. Geologické práce, Zprávy 34, 143-151 (in Slovak).

Hembree, D.I., Hasiotis, S.T., 2008. Miocene vertebrate and invertebrate burrows defining compound paleosols in the Pawnee Creek Formation, Colorado, U.S.A. Palaeogeography, Palaeoclimatology, Palaeoecology 270, 349-365.

Herbert, C.M., Alexander, J., Amos, K.J., Fielding, C.R., 2020. Unit bar architecture in a highly-variable fluvial discharge regime: Examples from the Burdekin River, Australia. Sedimentology 67, 576-605.

Hilgen, F.J., Lourens, L.J., Van Dam, J.A., 2012. The Neogene period. In: Gradstein, F.M., Ogg, J.G., Schmitz, M.D., Ogg, G. (Eds.), A Geologic Time Scale 2012. Elsevier, Amsterdam, pp. 923–978.

Holec, P., 1986. Neueste Resultate der Untersuchung von Neogenen und Quartären Nashörnern, Bären und Kleinsäugern in dem bereich der Westkarpaten (Slowakei). Acta Universitatis Carolinae – Geologica 2, 223-231 (in German).

Holec, P., 1996. A Plio-Pleistocene large mammal fauna from Strekov and Nová Vieska, south Slovakia. Acta Zoologia Cracoviensia 39, 1, 219-222.

Horváth, F., 1995. Phases of compression during the evolution of the Pannonian Basin and its bearing on hydrocarbon exploration. Marine and Petroleum Geology 12, 837-844.

Horváth, F., Bada, G., Szafián, P., Tari, G., Ádám, A., Cloetingh, S., 2006. Formation and deformation of the Pannonian Basin: Constraints from observational data, Geological Society Memoir, pp. 191-206.

Horváth, Z., Michéli, E., Mindszenty, A., Berényi-Üveges, J., 2005. Soft-sediment deformation structures in Late Miocene–Pleistocene sediments on the pediment of the Mátra Hills (Visonta, Atkár, Verseg): Cryoturbation, load structures or seismites? Tectonophysics 410, 81-95.

Chmeleff, J., von Blanckenburg, F., Kossert, K., Jakob, D., 2010. Determination of the $^{10}$Be half-life by multicollector ICP-MS and liquid scintillation counting. Nuclear Instruments and Methods in Physics Research, Section B: Beam Interactions with Materials and Atoms 268, 192-199.

Kahlke, R.-D., García, N., Kostopoulos, D.S., Lacombat, F., Lister, A.M., Mazza, P.P.A., Spassov, N., Titov, V.V., 2011. Western Palaearctic palaeoenvironmental conditions during the Early and early Middle Pleistocene inferred from large mammal communities, and implications for hominin dispersal in Europe. Quaternary Science Reviews 30, 1368-1395.

Knudsen, M.F., Nørgaard, J., Grischott, R., Kober, F., Egholm, D.L., Hansen, T.M., Jansen, J.D., 2020. New cosmogenic nuclide burial-dating model indicates onset of major glaciations in the Alps during Middle Pleistocene Transition. Earth and Planetary Science Letters 549.

Korschinek, G., Bergmaier, A., Faestermann, T., Gerstmann, U.C., Knie, K., Rugel, G., Wallner, A., Dillmann, I., Dollinger, G., von Gostomski, C.L., Kossert, K., Maiti, M., Poutivtsev, M., Remmert, A., 2010. A new value for the half-life of Be-10 by Heavy-Ion Elastic Recoil Detection and liquid scintillation counting. Nuclear Instruments &

Methods in Physics Research Section B-Beam Interactions with Materials and Atoms 268, 187-191.

Kovács, J., Szabó, P., Kocsis, L., Vennemann, T., Sabol, M., Gasparik, M., Virág, A., 2015. Pliocene and Early Pleistocene paleoenvironmental conditions in the Pannonian Basin (Hungary, Slovakia): Stable isotope analyses of fossil proboscidean and perissodactyl teeth. Palaeogeography, Palaeoclimatology, Palaeoecology 440, 455-466.

Kováč, M., Synak, R., Fordinál, K., Joniak, P., Tóth, C., Vojtko, R., Nagy, A., Baráth, I., Maglay, J., Minár, J., 2011. Late Miocene and Pliocene history of the Danube Basin: Inferred from development of depositional systems and timing of sedimentary facies changes. Geologica Carpathica 62, 519-534.

Ku, T.L., Kusakabe, M., Nelson, D.E., Southon, J.R., Korteling, R.G., Vogel, J., Nokikow, I., 1982. Constancy of oceanic deposition of $^{10}$Be as recorded in ferromanganese crusts. Nature 299, 240-242.

Lebatard, A.-E., Bourlès, D.L., Braucher, R., Arnold, M., Duringer, P., Jolivet, M., Moussa, A., Deschamps, P., Roquin, C., Carcaillet, J., Schuster, M., Lihoreau, F., Likius, A., Mackaye, H.T., Vignaud, P., Brunet, M., 2010. Application of the authigenic $^{10}$Be/$^{9}$Be dating method to continental sediments: Reconstruction of the Mio-Pleistocene sedimentary sequence in the early hominid fossiliferous areas of the northern Chad Basin. Earth and Planetary Science Letters 297, 57-70.

Lebatard, A.E., Bourlès, D.L., Duringer, P., Jolivet, M., Braucher, R., Carcaillet, J., Schuster, M., Arnaud, N., Monié, P., Lihoreau, F., Likius, A., Mackaye, H.T., Vignaud, P., Brunet, M., 2008. Cosmogenic nuclide dating of Sahelanthropus tchadensis and Australopithecus bahrelghazali: Mio-Pliocene hominids from Chad. Proceedings of the National Academy of Sciences of the United States of America 105, 3226-3231.

Leclair, S.F., Bridge, J.S., 2001. Quantitative interpretation of sedimentary structures formed by river dunes. Journal of Sedimentary Research 71, 713-716.

Li, S., Li, S., Shan, X., Gong, C., Yu, X., 2017. Classification, formation, and transport mechanisms of mud clasts. International Geology Review 59, 1609-1620.

Li, Z., Schieber, J., Pedersen, P.K., 2021. On the origin and significance of composite particles in mudstones: Examples from the Cenomanian Dunvegan Formation. Sedimentology 68, 737-754.

Long, D.G.F., Lowey, G.W., 2011. Wandering gravel-bed rivers and high-constructive stable channel sandy fluvial systems in the Ross River area, Yukon Territory, Canada. Geoscience Frontiers 2, 277-288.

Magyar, I., Geary, D.H., Müller, P., 1999. Paleogeographic evolution of the Late Miocene Lake Pannon in Central Europe. Palaeogeography, Palaeoclimatology, Palaeoecology 147, 151-167.

Magyar, I., Radivojevic, D., Sztano, O., Synak, R., Ujszaszi, K., Pocsik, M., 2013. Progradation of the paleo-Danube shelf margin across the Pannonian Basin during the Late Miocene and Early Pliocene. Global and Planetary Change 103, 168-173.

Martinetto, E., Monegato, G., Irace, A., Vaiani, S.C., Vassio, E., 2015. Pliocene and Early Pleistocene carpological records of terrestrial plants from the southern border of the Po Plain (northern Italy). Review of Palaeobotany and Palynology 218, 148-166.

Merchel, S., Braucher, R., Lachner, J., Rugel, G., 2021. Which is the best 9Be carrier for $^{10}Be/^{9}Be$ accelerator mass spectrometry? MethodsX 8.

Merchel, S., Herpers, U., 1999. An Update on Radiochemical Separation Techniques for the Determination of Long-Lived Radionuclides via Accelerator Mass Spectrometry. Radiochimica Acta 84, 215-220.

Miall, A.D., 2006. The geology of fluvial deposits: Sedimentary facies, basin analysis, and petroleum geology, 3rd edition ed. Springier, Berlin.

Milán, J., Theodorou, G., Loope, D.B., Panayides, I., Clemmensen, L.B., Gkioni, M., 2015. Vertebrate tracks in late pleistocene-early holocene (?) carbonate aeolianites, paphos, cyprus. Annales Societatis Geologorum Poloniae 85, 507-514.

Mulder, T., Alexander, J., 2001. The physical character of subaqueous sedimentary density flow and their deposits. Sedimentology 48, 269-299.

Müller, R., Nystuen, J.P., Wright, V.P., 2004. Pedogenic mud aggregates and paleosol development in ancient dryland river systems: Criteria for interpreting alluvial mudrock origin and floodplain dynamics. Journal of Sedimentary Research 74, 537-551.

Murton, J.B., Worsley, P., Gozdzik, J., 2000. Sand veins and wedges in cold aeolian environments. Quaternary Science Reviews 19, 899-922.

Muttoni, G., Carcano, C., Garzanti, E., Ghielmi, M., Piccin, A., Pini, R., Rogledi, S., Sciunnach, D., 2003. Onset of major Pleistocene glaciations in the Alps. Geology 31, 989-992.

Nadon, G., Tanke, D., Carpenter, K., 2001. The impact of sedimentology on vertebrate track studies. Mesozoic vertebrate life, 395-407.

Naqshband, S., Hoitink, A.J.F., McElroy, B., Hurther, D., Hulscher, S.J.M.H., 2017. A Sharp View on River Dune Transition to Upper Stage Plane Bed. Geophysical Research Letters 44, 11,437-411,444.

Noack, M., Gerbersdorf, S.U., Hillebrand, G., Wieprecht, S., 2015. Combining Field and Laboratory Measurements to Determine the Erosion Risk of Cohesive Sediments Best. Water 7, 5061-5077.

Novello, A., Lebatard, A.E., Moussa, A., Barboni, D., Sylvestre, F., Bourlès, D.L., Paillès, C., Buchet, G., Decarreau, A., Duringer, P., Ghienne, J.F., Maley, J., Mazur, J.C., Roquin, C., Schuster, M., Vignaud, P., 2015. Diatom, phytolith, and pollen records from a

$^{10}$Be/$^{9}$Be dated lacustrine succession in the chad basin: Insight on the miocene-pliocene paleoenvironmental changes in Central Africa. Palaeogeography, Palaeoclimatology, Palaeoecology 430, 85-103.

Paquette, J.-L., Médard, E., Poidevin, J.-L., Barbet, P., 2021. Precise dating of middle to late Villafranchian mammalian paleofaunae from the Upper Allier River valley (French Massif Central) using U–Pb geochronology on volcanic zircons. Quaternary Geochronology 65, 101198.

Perkey, D.W., Smith, S.J., Fall, K.A., Massey, G.M., Friedrichs, C.T., Hicks, E.M., 2020. Impacts of Muddy Bed Aggregates on Sediment Transport and Management in the Tidal James River, VA. Journal of Waterway, Port, Coastal, and Ocean Engineering 146, 04020028.

Raffi, I., Wade, B.S., Pälike, H., Beu, A.G., Cooper, R., Crundwell, M.P., Krijgsman, W., Moore, T., Raine, I., Sardella, R., Vernyhorova, Y.V., 2020. The Neogene Period. Gradstein, F.M., Ogg, J.G., Schmitz, M.D., Ogg, G.M., (Eds.), Geologic Time Scale 2020. Elsevier, 1141-1215.

Raisbeck, G.M., Yiou, F., Fruneau, M., Loiseaux, J.M., Lievin, M., Ravel, J.C., 1981. Cosmogenic $^{10}$Be/$^{7}$Be as a probe of atmospheric transport processes. Geophysical Research Letters 8, 1015-1018.

Reesink, A.J.H., 2018. Interpretation of cross strata formed by unit bars, In: Ghinassi, M., Colombera, L., Mountney, N.P., Reesink, A.J.H. (Eds.), Fluvial Meanders and Their Sedimentary Products in the Rock Record. International Association of Sedimentologists Special Publication, Wiley-Blackwell, Oxford, pp. 173-200.

Reesink, A.J.H., Bridge, J.S., 2011. Evidence of bedform superimposition and flow unsteadiness in unit-bar deposits, South Saskatchewan river, Canada. Journal of Sedimentary Research 81, 814-840.

Rook, L., Martínez-Navarro, B., 2010. Villafranchian: The long story of a Plio-Pleistocene European large mammal biochronologic unit. Quaternary International 219, 1-2, 134-144.

Ruszkiczay-Rüdiger, Z., Balázs, A., Csillag, G., Drijkoningen, G., Fodor, L., 2020. Uplift of the Transdanubian Range, Pannonian Basin: How fast and why? Global and Planetary Change 192.

Ruszkiczay-Rüdiger, Z., Csillag, G., Fodor, L., Braucher, R., Novothny, Á., Thamó-Bozsó, E., Virág, A., Pazonyi, P., Timár, G., 2018. Integration of new and revised chronological data to constrain the terrace evolution of the Danube River (Gerecse Hills, Pannonian Basin). Quaternary Geochronology 48, 148-170.

Ruszkiczay-Rüdiger, Z., Kern, Z., 2016. Permafrost or seasonal frost? A review of paleoclimate proxies of the last glacial cycle in the East Central European lowlands. Quaternary International 415, 241-252.

Schaller, M., Lachner, J., Christl, M., Maden, C., Spassov, N., Ilg, A., Böhme, M., 2015. Authigenic Be as a tool to date river terrace sediments? – An example from a Late Miocene hominid locality in Bulgaria. Quaternary Geochronology 29, 6-15.

Schieber, J., 1998. Shales and Mudstones, In: Schieber, J., Zimmerle, W., Sethi, P.S. (Eds.), I. Basin Studies, Sedimentology and Paleontology. Schweizerbart, Stuttgart, pp. 131-146.

Schieber, J., 2016. Mud re-distribution in epicontinental basins - Exploring likely processes. Marine and Petroleum Geology 71, 119-133.

Schieber, J., Southard, J.B., Schimmelmann, A., 2010. Lenticular shale fabrics resulting from intermitent erosion of water-rich muds - Interpreting the rock record in the light of recent flume experiments. Journal of Sedimentary Research 80, 119-128.

Schmidt, Z., 1977. Geographical extension of archidiscodonts in Slovakia. Západné Karpaty, séria paleontológia 3-2, 233-240.

Schmidt, Z., Halouzka, R., 1970. Nová fauna villafranchienu zo Strekova na Hronskej pahorkatine (Podunajská nížina). Geologické práce, Správy, 51, 173-183 (in Slovak).

Simon, Q., Ledru, M.P., Sawakuchi, A.O., Favier, C., Mineli, T.D., Grohmann, C.H., Guedes, M., Bard, E., Thouveny, N., Garcia, M., Tachikawa, K., Rodríguez-Zorro, P.A., 2020. Chronostratigraphy of a 1.5±0.1 Ma composite sedimentary record from Colônia basin (SE Brazil): Bayesian modeling based on paleomagnetic, authigenic $^{10}Be/^{9}Be$, radiocarbon and luminescence dating. Quaternary Geochronology 58.

Smith, J.J., Hasiotis, S.T., Woody, D.T., Kraus, M.J., 2008. Paleoclimatic implications of crayfish-mediated prismatic structures in paleosols of the Paleogene Willwood Formation, Bighorn Basin, Wyoming, U.S.A. Journal of Sedimentary Research 78, 323-334.

Spencer, C.J., Yakymchuk, C., Ghaznavi, M., 2017. Visualising data distributions with kernel density estimation and reduced chi-squared statistic. Geoscience Frontiers 8, 1247-1252.

Stow, D.A., 2005. Sedimentary Rocks in the Field. A Colour Guide. Manson Publishing, London.

Sztanó, O., Kováč, M., Magyar, I., Šujan, M., Fodor, L., Uhrin, A., Rybár, S., Csillag, G., Tokés, L., 2016. Late Miocene sedimentary record of the Danube/Kisalföld Basin: Interregional correlation of depositional systems, stratigraphy and structural evolution. Geologica Carpathica 67, 525-542.

Šujan, M., Braucher, R., Kováč, M., Bourlès, D.L., Rybár, S., Guillou, V., Hudáčková, N., 2016. Application of the authigenic $^{10}Be/^{9}Be$ dating method to Late Miocene–Pliocene sequences in the northern Danube Basin (Pannonian Basin System): Confirmation of heterochronous evolution of sedimentary environments. Global and Planetary Change 137, 35-53.

Šujan, M., Braucher, R., Rybár, S., Maglay, J., Nagy, A., Fordinál, K., Šarinová, K., Sýkora, M., Józsa, Š., Kováč, M., 2018. Revealing the late Pliocene to Middle Pleistocene alluvial archive in the confluence of the Western Carpathian and Eastern Alpine rivers: $^{26}$Al/$^{10}$Be burial dating from the Danube Basin (Slovakia). Sedimentary Geology 377, 131-146.

Šujan, M., Braucher, R., Tibenský, M., Fordinál, K., Rybár, S., Kováč, M., 2020. Effects of spatially variable accommodation rate on channel belt distribution in an alluvial sequence: Authigenic $^{10}$Be/$^{9}$Be-based Bayesian age-depth models applied to the upper Miocene Volkovce Fm. (northern Pannonian Basin System, Slovakia). Sedimentary Geology 397, 105566.

Šujan, M., Rybár, S., 2014. The development of Pleistocene river terraces in the eastern part of the Danube Basin. Acta Geologica Slovaca 6, 107-122 (in Slovak with English summary).

Šujan, M., Rybár, S., Kováč, M., Bielik, M., Majcin, D., Minár, J., Plašienka, D., Nováková, P., Kotulová, J., 2021. The polyphase rifting and inversion of the Danube Basin revised. Global and Planetary Change 196, 103375.

Tari, G., 1994. Alpine tectonics of the Pannonian Basin. PhD. Thesis, Rice University, Houston.

Tari, G., Arbouille, D., Schléder, Z., Tóth, T., 2020. Inversion tectonics: A brief petroleum industry perspective. Solid Earth 11, 1865-1889.

Teodoridis, V., Bruch, A.A., Vassio, E., Martinetto, E., Kvaček, Z., Stuchlik, L., 2017. Plio-Pleistocene floras of the Vildštejn Formation in the Cheb Basin, Czech Republic — A floristic and palaeoenvironmental review. Palaeogeography, Palaeoclimatology, Palaeoecology 467, 166-190.

Toonen, W.H.J., Kleinhans, M.G., Cohen, K.M., 2012. Sedimentary architecture of abandoned channel fills. Earth Surface Processes and Landforms 37, 459-472.

Vakarcs, G., Vail, P.R., Tari, G., Pogácsás, G., Mattick, R.E., Szabó, A., 1994. Third-order Middle Miocene-Early Pliocene depositional sequences in the prograding delta complex of the Pannonian Basin. Tectonophysics 240, 81-106.

Van Husen, D., 2004. Quaternary glaciations in Austria, Developments in Quaternary Sciences. Elsevier, pp. 1-13.

Van Rijn, L.C., 2020. Erodibility of Mud-Sand Bed Mixtures. Journal of Hydraulic Engineering 146.

van Vliet-Lanoë, B., Magyari, A., Meilliez, F., 2004. Distinguishing between tectonic and periglacial deformations of quaternary continental deposits in Europe. Global and Planetary Change 43, 103-127.

Vandenberghe, J., 2013. Cryoturbation Structures, Encyclopedia of Quaternary Science: Second Edition, pp. 430-435.

Vlačiky, M., 2009: Výskumy kvartérnych paleontologických lokalít na Slovensku v roku 2009. In: Németh, Z., Plašienka, D., Šimon, L., Kohút, M., Iglárová, Ľ., (Eds.), 8. výročný predvianočný seminár SGS. Nové poznatky o stavbe a vývoji Západných Karpát. Mineralia Slovaca, Geovestník, ŠGÚDŠ, Bratislava, 41, 4, 549-550 (in Slovak).

Vlačiky, M., Moravcová, M., Ďurišová, A., Krupa., V., 2009. Výskumy kvartérnych paleontologických lokalít na Slovensku v roku 2009. In: Ivanov M., Roszková A., Sedláček, J., Šimíček, D., (Eds.) 15. Kvartér 2009. Sborník abstrakt, ÚGV PřF MU, ČGS, Brno, 35-36 (in Slovak).

Vlačiky, M., Moravcová, M., Maglay, J., Zervanová, J., Joniak, P., Tóth, Cs., 2010. Pokračovanie výskumu plio-pleistocénnej lokality Nová Vieska (SR) v roku 2010. In: Dohnalová, A., Uhlířová, H., (Eds.), 16. Kvartér 2010. Sborník abstrakt, ÚGV PřF MU, ČGS, Brno, 29-30 (in Slovak).

Vlačiky, M., Sliva, Ľ., Tóth, C., Karol, M., Zervanová, J., 2008. The fauna and sedimentology of the locality Nová Vieska (Villafranchian, SR). Acta Musei Moraviae, Scientiae geologicae 93, 229-244.

Vlačiky, M., Šujan, M., Rybár, S., Braucher, R., 2017. Nová Vieska locality: fauna, sediments and their dating – new results, 15th predvianočný geologický seminár SGS – Nové poznatky o stavbe a vývoji Západných Karpát, Mente et Maleo, Abstracts, p. 57.

Vlačiky, M., Tóth, Cs., Šujan, M., Rybár, S., Zervanová, J., Sakala, J., 2013. Najnovšie výsledky výskumu hranice pliocén/pleistocén v sedimentoch Podunajskej nížiny. In: Uhlířová, H., Malíková, R., Ivanov, M., (Eds.), 19. Kvartér 2013. Sborník abstrakt, ÚGV PřF MU, ČGS, Brno, 73-74 (in Slovak).

Willenbring, J.K., von Blanckenburg, F., 2010. Meteoric cosmogenic Beryllium-10 adsorbed to river sediment and soil: Applications for Earth-surface dynamics. Earth-Science Reviews 98, 105-122.

Wittmann, H., Von Blanckenburg, F., Bouchez, J., Dannhaus, N., Naumann, R., Christl, M., Gaillardet, J., 2012. The dependence of meteoric $^{10}$Be concentrations on particle size in Amazon River bed sediment and the extraction of reactive $^{10}$Be/$^{9}$Be ratios. Chemical Geology 318-319, 126-138.

Wittmann, H., von Blanckenburg, F., Mohtadi, M., Christl, M., Bernhardt, A., 2017. The competition between coastal trace metal fluxes and oceanic mixing from the $^{10}$Be/$^{9}$Be ratio: Implications for sedimentary records. Geophysical Research Letters 44, 8443-8452.

Yawar, Z., Schieber, J., 2017. On the origin of silt laminae in laminated shales. Sedimentary Geology 360, 22-34.

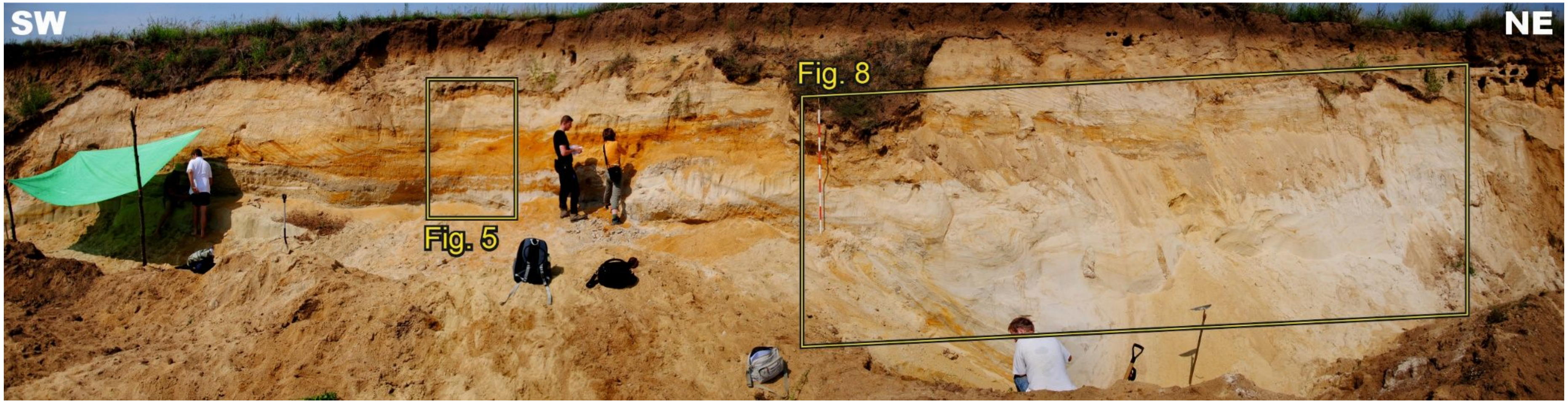


Suppl. Fig. 1. A panoramic photograph for correlation of the Figs. 5 and 8.